Paleoceanography and Paleoclimatology

RESEARCH ARTICLE
10.1029/2023PA004777

Key Points:

- Northwest African monsoon intensity declined substantially sometime between 1.0 and 0.5 Ma
- Rainfall penetration or disturbances may be more consequential than monsoon strength for ecosystem biogeography over 10^5–10^6 years
- Sedimentary dust and opal fluxes drop following monsoon intensity decline, linking dust production, dust flux, and marine productivity

Supporting Information:

Supporting Information may be found in the online version of this article.

Correspondence to:

N. A. O'Mara and P. J. Polissar,
nicholas.omara@yale.edu;
ppolissar@ucsc.edu

Citation:

O'Mara, N. A., Skonieczny, C., McGee, D., Winckler, G., Bory, A. J.-M., Bradtmiller, L. I., et al. (2024). Constraining Plio-Pleistocene shifts in Northwest African hydroclimate, ecosystem distributions, and marine productivity: New paleo-records across the Mid-Pleistocene Transition. *Paleoceanography and Paleoclimatology*, *39*, e2023PA004777. https://doi.org/10.1029/2023PA004777

Received 3 OCT 2023
Accepted 15 MAY 2024

Author Contributions:

Conceptualization: Nicholas A. O'Mara, Charlotte Skonieczny, David McGee, Gisela Winckler, Pratigya J. Polissar
Formal analysis: Nicholas A. O'Mara, Charlotte Skonieczny, Gisela Winckler, Louisa I. Bradtmiller, Pratigya J. Polissar
Funding acquisition: David McGee, Gisela Winckler, Pratigya J. Polissar
Investigation: Nicholas A. O'Mara, Charlotte Skonieczny, David McGee, Gisela Winckler, Aloys J.-M. Bory, Louisa I. Bradtmiller, Bruno Malaizé, Pratigya J. Polissar
Methodology: Nicholas A. O'Mara, Pratigya J. Polissar
Resources: Bruno Malaizé
Supervision: David McGee, Gisela Winckler, Pratigya J. Polissar

Constraining Plio-Pleistocene Shifts in Northwest African Hydroclimate, Ecosystem Distributions, and Marine Productivity: New Paleo-Records Across the Mid-Pleistocene Transition

Nicholas A. O'Mara[1,2,3,4], Charlotte Skonieczny[5], David McGee[6], Gisela Winckler[1,2], Aloys J.-M. Bory[7], Louisa I. Bradtmiller[8], Bruno Malaizé[9], and Pratigya J. Polissar[10]

[1]Lamont-Doherty Earth Observatory, Columbia University, Palisades, NY, USA, [2]Department of Earth and Environmental Sciences, Columbia University, New York, NY, USA, [3]Now at Yale Institute for Biospheric Studies, Yale University, New Haven, CT, USA, [4]Now at Yale School of the Environment, Yale University, New Haven, CT, USA, [5]Université Paris-Saclay, CNRS, GEOPS, Orsay, France, [6]Department of Earth, Atmospheric and Planetary Sciences, Massachusetts Institute of Technology, Cambridge, MA, USA, [7]Laboratoire d'Océanologie et de Géosciences, Université de Lille, CNRS, Université Littoral Cote d'Opale, UMR 8187, LOG, Lille, France, [8]Department of Environmental Studies, Macalester College, St. Paul, MN, USA, [9]UMR CNRS 5805 EPOC, Université Bordeaux I, Talence, France, [10]Ocean Sciences Department, University of California, Santa Cruz, CA, USA

Abstract Northwest Africa transitioned from a wet/vegetated landscape toward drier/sparser conditions sometime between the late-Pliocene and the late-Pleistocene. However, our understanding of the precise timing and nature of this transition is hampered by a paucity of paleo-records which bridge these two intervals. Here we report new plant-wax isotope as well as dust and opal flux records from the relatively brief interval ~1.1–1.0 million years ago (Ma) to evaluate the astronomical timescale controls of Northwest African hydroclimate and vegetation during the Mid-Pleistocene Transition (MPT) and, in context with published records, the drivers of long-term climate and ecological trends over the Plio-Pleistocene. The tempo and amplitude of the Northwest African monsoon rainfall swings closely track low latitude insolation forcings over the last 5 Ma. However, we demonstrate that a pronounced mean state decline in monsoon strength likely occurred following the MPT most likely instigated by increasing Atlantic meridional sea surface temperature gradients or declines in the strength of the meridional overturning circulation. The northward extent of vegetation does not track changes in monsoon strength over the Plio-Pleistocene and thus may be more strongly influenced by changes in monsoon rainfall extent or ecosystem disturbances. Progressively diminished dust fluxes following a decline in monsoon strength after 1.0 Ma is consistent with reduced production and subsequent depletion of fine-grained sediments in the Sahara. Synchroneity between dust and opal fluxes across timescales suggests nutrient delivery to the surface ocean via dust plays a key role in marine primary productivity off the coast of Northwest Africa.

1. Introduction

The Sahara is the most expansive hot desert on Earth and is the largest source of dust to the atmosphere and the world's oceans (Ginoux et al., 2012). Moving north to south, barren desert landscapes transition to grassland, savanna, and forest ecosystems where increasing woody cover is facilitated by rising rates of seasonal monsoonal precipitation. On time scales of thousands of years, paleoproxy records of terrestrial vegetation from pollen and plant biomarkers reveal that the spatial distribution and composition of these biomes have varied dramatically in response to past climate forcings. For example, during the African Humid Period (AHP), ca. 14.5–5.5 thousand years ago (ka), increased monsoonal precipitation yielded northward expansions of grasslands, savannas, and, to a lesser extent, forests across what today is a desert landscape (Dallmeyer et al., 2020; Hély et al., 2014; Jolly et al., 1998; Ritchie et al., 1985). Declines in dust and opal fluxes to marine sediments concomitant with these rainfall and vegetation shifts demonstrate the strong connection between monsoon strength, dust production/transport, and surface ocean primary productivity along the Northwest African margin (Bradtmiller et al., 2016; McGee et al., 2013). The AHP is not a unique event, but the most recent iteration of stronger than normal monsoon conditions in North Africa long postulated to have resulted from astronomical forcing associated with variations in the Earth's axial tilt and orbit about the sun (Kutzbach, 1981; Tuenter et al., 2005). In recent years, multiple lines of paleo-proxy evidence (Crocker et al., 2022; Hennekam et al., 2022; Kuechler et al., 2018;

Writing – original draft: Nicholas A. O'Mara
Writing – review & editing: Nicholas A. O'Mara, Charlotte Skonieczny, David McGee, Gisela Winckler, Aloys J.-M. Bory, Louisa I. Bradtmiller, Bruno Malaizé, Pratigya J. Polissar

Larrasoaña, 2021; O'Mara et al., 2022; Skonieczny et al., 2019) and climate models (Bosmans, Drijfhout, et al., 2015; Bosmans, Hilgen, et al., 2015; Mantsis et al., 2014; Rachmayani et al., 2016) alike have begun to converge on specific astronomical drivers of the magnitude and tempo of such variations in North African hydroclimate via changes in the strength of the West African monsoon. These paleorecords and simulations show that the amount of monsoon rainfall is enhanced both when local insolation is high and when there is a strong insolation gradient between southern and northern hemisphere tropics. Mechanistically, increased local insolation strengthens the monsoon by increasing convective activity over Northwest Africa, while stronger insolation gradients across the equator result in enhanced moisture transport into the monsoon region from the subtropical North Atlantic and equatorial Atlantic Ocean (Bosmans, Drijfhout, et al., 2015). These insolation changes are controlled by the precession (19/23 kyr period) and obliquity (41 kyr period) of the Earth's orbit and have been acting as pacemakers for Northwest African wet/dry cycles (Rossignol-Strick, 1983, 1985) for at least the last 11 Myr (Crocker et al., 2022).

Despite continuous astronomical pacing of the monsoons, on timescales of hundreds of thousands to millions of years, monsoon strength and ecosystem distributions exhibit secular shifts that cannot be explained by astronomical variability. Under the backdrop of stationary astronomical forcing over the last 5 million years, Northwest African monsoon strength has declined, and vegetation zones have shifted southward giving way to a more expansive Sahara (de Menocal, 1995; Leroy & Dupont, 1994; Novello et al., 2015; Ruddiman et al., 1989; Vallé et al., 2014). The mechanisms within the climate system which govern monsoon strength on astronomical timescales therefore appear disconnected from those that govern longer-term shifts. However, the timing of these shifts as well as their character (i.e., gradual vs. abrupt) are not well constrained in the paleo-record, hampering our ability to test hypothesized long-term drivers of monsoon strength, terrestrial biogeography, dust emissions to the atmosphere/ocean, and marine productivity.

Here we explore the drivers of the Northwest African late-Pleistocene monsoon and ecosystem changes with new marine sediment core data from a 100 kyr interval within the MPT (1.1–1.0 Ma). We use plant-wax hydrogen isotopes (δD) to reconstruct monsoon rainfall intensity and plant-wax carbon isotopes ($\delta^{13}C$) to record changes in vegetation. We also compute constant flux normalized dust and opal fluxes using the $^{3}He_{ET}$-normalization technique to investigate how changes in monsoon strength and regional vegetation conditions impact marine dust fluxes and productivity. We investigate these proxies both individually and in concert and compare the results with previous estimates from the same or proximal marine records for a series of snapshots across the Plio-Pleistocene.

2. Background

Within North Africa, the physical ocean-land-atmosphere processes which control West African monsoon intensity also impact and feedback with terrestrial vegetation distributions, wind strength/direction, dust emissions, and marine productivity on annual to astronomical (10^4 yr) timescales (Bradtmiller et al., 2016; Chandan & Peltier, 2020; Claussen et al., 2017; Kutzbach et al., 1996; McGee et al., 2013; Pausata et al., 2016). In this study, we use the uniquely long histories of climate and environmental change provided by marine sediment core records to examine how the various components of this system have or have not differentially responded to changes in the Earth's climate and test various hypotheses for what may be driving observed long-term shifts. To do so, we generate new paleo-records during a 100 kyr time slice (1.1–1.0 Ma) within the extended MPT (~1.2–0.8 Ma) when global glaciations became more intense and increased in duration (Pisias & Moore, 1981). In this section, we review the modern climate system and provide the paleoclimatic context within which we will interpret our new data.

2.1. Regional Setting

Modern Northwest African vegetation zones primarily track changes in precipitation (White, 1983). North of the Sahara, forest and steppe environments comprise the principally winter precipitation-fed Mediterranean ecosystems. Vegetation cover declines to the south as precipitation wanes giving way to the sparsely vegetated Sahara delineated by mean annual precipitation rates less than 100 mm/yr. At the southern fringe of the Sahara, higher and increasingly seasonal precipitation caused by intense monsoonal rainfall during the summer months (July–September) supports Sahelian grassland ecosystems. Precipitation continues to rise southward resulting in correspondingly verdant vegetation including Sudanian savannas, Guinean deciduous forests, and the Guineo-

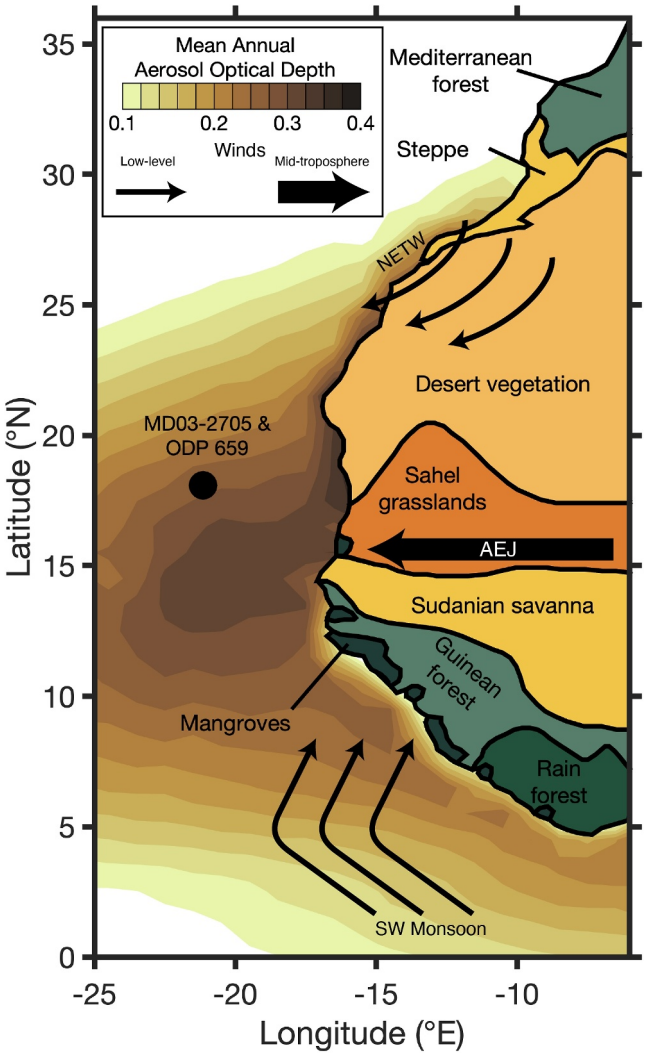

Figure 1. Regional setting. The modern distribution of biomes, prevailing wind patterns, and the modern Saharan Dust plume. Biome distributions are from Hooghiemstra et al. (2006). Mean annual dust-specific aerosol optical depth (2001–2018) (Voss & Evan, 2020). The black circle indicates marine sediment cores MD03-2705 and ODP 659. Black arrows schematically show the direction and atmospheric level of the Northeast Trade Winds (NETW), the African Easterly Jet (AEJ), and the Southwesterly monsoon flow (SW Monsoon).

Congolian rain forests (White, 1983) (Figure 1). Within the broader constraints established by precipitation gradients and rainfall seasonality, ecosystem disturbances (e.g., by herbivory and fire) are also important determiners of both biome distributions and vegetation structure within ecosystems (Archibald & Hempson, 2016; Bond et al., 2005; Sankaran et al., 2005).

Northwest Africa is under the influence of three major wind systems which impact both material fluxes from the African continent to the ocean and marine productivity via coastal upwelling (Fischer et al., 2016). The dry northeasterly trade (or Harmattan) winds blow year-round in the near surface across the Sahara toward the West African monsoon region. Southwesterly monsoon winds—most active during the summer monsoon season (JJAS)—blow toward the northeast delivering moisture to the African interior. These two surface winds oppose each other and converge at ~20°N, in a region sometimes referred to as the Intertropical Convergence Zone (ITCZ). However, due to persisting confusion conflating the ITCZ with the zone of maximum rainfall over continents, this terminology applied over land, especially over Africa is inadvisable (Nicholson, 2018). Regardless of moniker, the shallow convection at this convergence can only spur limited rainfall during the summer months; the core region of monsoon rainfall in fact occurs ~1,000 km to the south. The tropical rainbelt (centered on ~10°N) is situated between the axes of the zonally flowing mid-tropospheric African Easterly Jet (AEJ) and the aloft Tropical Easterly Jet (TEJ). In this zonal band, deep convection co-occurs with moisture transported from the eastern Atlantic by the low-level West African Westerly Jet (WAWJ) (over the ocean) (Grodsky et al., 2003; Pu & Cook, 2010) and the African Westerly Jet (AWJ) (over the continent) (Grist & Nicholson, 2001) producing a regional maximum in summer monsoon rainfall. Slightly farther south (~5°N), a third coastal convection cell associated with sea-breeze effects from the eastern equatorial Atlantic converges with the core tropical rainbelt convective cell delivering a modest amount of moisture and limited rainfall (Nicholson, 2008, 2009).

In addition to shaping hydrological conditions over Northwest Africa, the transport of terrestrial material (e.g., dust, pollen, plant waxes, etc) from Northwest Africa to the eastern North Atlantic Ocean is largely controlled by these wind systems, namely the low-level northeasterly trades (Harmattans) and the mid-level AEJ. During the summer the AEJ mainly transports terrestrial material westward at mid-tropospheric altitudes within the Saharan Air Layer (SAL) to the North Atlantic Ocean as far as the Caribbean (Prospero, 1999; Prospero & Carlson, 1972). Winter and spring Harmattan winds—more precisely outbreak events during these seasons—are the most important suppliers of dust to the Northwest African margin (Skonieczny et al., 2013; van der Does et al., 2020). These mineral dusts are composed of silt and clay particles originating primarily from the Northwest Sahara (Morocco, Mauritania, Mali, Algeria) with minor contributions from the Central Sahara (Niger, Libya, Chad) (Le Quilleuc et al., 2021; Skonieczny et al., 2011, 2013; Stuut et al., 2005) (See Text S6 in Supporting Information S1 for further discussion). Dust deposition and wind-driven coastal upwelling both add nutrients to the surface ocean, contributing to high primary productivity in the Canary Current system that runs southward along the Northwest African coast (Fischer, Karakas, et al., 2009; Fischer, Reuter, et al., 2009; Fischer et al., 2016, 2019; Ohde & Siegel, 2010). Plant waxes delivered to this oceanic area are primarily from the sub-Saharan Sahelian grassland, Sudanian savanna, and Guinean deciduous forest ecosystems (Figure 1) (Schefuß et al., 2003) and record landscape vegetation composition in marine sediments (Huang et al., 2000). Through comparison of pollen and plant wax isotope values O'Mara et al. (2022) demonstrated that steppe and Mediterranean forest ecosystems north of the Sahara were not an important source of plant waxes.

Rainfall regimes across North Africa are spatially heterogenous, owing to the myriad influences of atmospheric processes, topographic factors, as well as ocean/atmosphere dynamics stemming from multiple oceans which operate over a wide range of spatial scales. In general, North Africa can be divided into three main rainfall regimes: (a) the Mediterranean regions characterized by warm dry summers and cool wet winters which dominate north of the Sahara, (b) the West African monsoon region south of the Sahara from the Sahel to the Gulf of Guinea and from the Atlantic to roughly 30°E characterized by warm wet summers and cool dry winters, and (c) the region East of 30°E where the high topography of the Ethiopian highlands and the East African rift delineate the East African monsoon region characterized by a bimodal rainy season and a much stronger Indian Ocean influence on rainfall (Nicholson, 2013, 2018; Nicholson et al., 2018). However, within region (b), generally referred to as North Africa, modern meteorological studies reveal that the Sahel generally has two distinct rainfall regimes, the western coastal region and a central region demarcated by the 10°W meridian (Lebel & Ali, 2009; Nicholson, 1980; Nicholson & Palao, 1993) likely owing to zonal asymmetries in the Saharan Heat Low (Biasutti, 2019; Lavaysse et al., 2010) or independent interannual variability of the AEJ and TEJ (Nicholson, 2013). Therefore, throughout this study, we refer to region (b) as a whole as North Africa, while we refer to the western sector of this region (west of 10°W), the dominant source area of the waxes and dust to our core site, as Northwest Africa. Analogously, we distinguish the western most region of the West African monsoon as the Northwest African monsoon.

2.2. Paleoclimatic Context

Compared to the late-Pleistocene, during the Pliocene, 5.33–2.58 Ma, global temperatures were higher (Fedorov et al., 2013; Haywood et al., 2013, 2020; Westerhold et al., 2020), atmospheric CO_2 concentrations were higher (Cenozoic CO2 Proxy Integration Project (CenCO2PIP) Consortium et al., 2023; Pagani et al., 2010), and global precipitation was higher (especially in the subtropics) (Burls & Fedorov, 2017; Haywood et al., 2020). In North Africa specifically, paleo-proxy records of biogeography and hydrology (Cerling et al., 1997; Feakins et al., 2013; Leroy & Dupont, 1994; Novello et al., 2015; Ruddiman et al., 1989; Vallé et al., 2014) and climate models (Berntell et al., 2021; Salzmann et al., 2008; Zhang et al., 2019) agree that landscapes were much wetter and more vegetated with a significantly smaller Sahara. Long and continuous archives of dust flux to sediments along the West African margin provided the first estimates of the development of continental aridity in North Africa over the Plio-Pleistocene. Stepwise increases of dust fluxes at ∼2.8, ∼1.7, and ∼1.0 Ma were interpreted as declines in monsoon strength caused by expansions of Northern Hemisphere ice volume (de Menocal, 1995, 2004; Tiedemann et al., 1994). Similar increases in dust fluxes to North Pacific (Abell et al., 2021, 2023; Bridges et al., 2023; Rea et al., 1998), South Atlantic (Martínez-Garcia et al., 2011), North Atlantic (Crocker et al., 2022; Naafs et al., 2012) marine sediments broadly coeval with the timing inception of Northern Hemisphere glaciation (iNHG) reveal this increase in dustiness may have been a global phenomenon. However, the degree to which secular shifts in dust fluxes as well as their temporal trends are controlled by changes in hydroclimate, wind strength/positioning, and dust source region characteristics remains unclear. Recent work, using constant flux proxy techniques (CFPs) such as $^{230}Th_{XS}$-normalization in Northwest African margin sediments showed that enhanced calcium carbonate dissolution during glacial periods causes spuriously high dust fluxes (Skonieczny et al., 2019). Moreover, in the North Pacific, long-term trends in dust flux across the Pleistocene calculated using traditional dust flux records versus CFP methods ($^{3}He_{ET}$-normalization) are at odds (Abell et al., 2023). Thus, in the North African context, previously reported increased dust fluxes in Northwest African margin sediments during times of expanding ice sheets may have resulted from methodological artifacts rather than increased continental aridity. Constant-flux dust records only extend back ∼500 kyr, thus the long-term evolution of the connection between Northwest African dust and hydroclimate remain uncertain.

Paleo-proxy records sensitive to various aspects of North African aridity yield conflicting timelines for regional Plio-Pleistocene hydroclimate evolution. Bulk elemental ratios from Northwest African margin sediments, which record the degree of soil weathering in dust source regions and the relative abundance of riverine clays in terrestrial dust, show precession (19/23 kyr) and obliquity (41 kyr) variability as far back as 11 Ma (Crocker et al., 2022). These records are also characterized by shifts toward more weathered and less riverine clay-rich dust sources nearly concurrent with the iNHG (∼3.1 and ∼2.7 Ma respectively). This suggests that the initial development of Northern Hemisphere ice sheets may have indeed driven aridification in North Africa. In contrast, factorial climate model simulations isolating the impacts of astronomical, greenhouse gas (GHG), and ice sheet forcing since 190 thousand years ago (ka) show a strong control of astronomical forcing on hydroclimate and

vegetation greening in the Sahara with little influence from GHGs and ice sheets (Duque-Villegas et al., 2022). However, these simulations explore variations in these parameters between late-Pleistocene glacial and interglacial conditions, so it is unclear how a state change from little to no permanent Northern Hemisphere ice sheets, to large permanent ice sheets may have impacted North African aridity across the iNHG. Other proxy data including increasing dust fluxes and decreased occurrences of sapropel deposits in the Mediterranean Sea (Almogi-Labin, 2011; Grant et al., 2022; Hennekam et al., 2022; Larrasoaña et al., 2003) as well as shifts toward more drought-tolerant taxa in central Africa (Dupont et al., 2001; Schefuß et al., 2003) in fact suggest a much later timing of African aridification that more closely corresponds with the Mid-Pleistocene transition (MPT; 1.2–0.8 Ma). While these proxy data are related to changes in rainfall, they are all secondary recorders of hydroclimate.

The hydrogen and carbon isotopic composition of plant epicuticular waxes preserved in marine sediments provide some of the best direct proxy evidence for regional scale hydroclimate and vegetation compositional changes. In North Africa, the hydrogen isotopic composition of rainfall (δD_{Precip}) is highly correlated with mean annual precipitation amount as precipitation becomes progressively isotopically lighter with increasing cumulative rainfall (Dansgaard, 1964; Niedermeyer et al., 2016; Rozanski et al., 1993). Plants use precipitated water as their main hydrogen source incorporating the δD_{Precip} into the waxes they produce (Sachse et al., 2012) thus allowing for quantitative reconstructions of monsoon strength. Likewise for carbon isotopes, the C source for plants is atmospheric CO_2. Unlike water vapor, CO_2 is well mixed in the atmosphere so $\delta^{13}C_{CO2}$ is relatively spatially uniform. Instead, the carbon isotopic signature of waxes ($\delta^{13}C_{wax}$) is predominantly determined by plant photosynthetic strategy where C_3 plants discriminate more strongly against heavy ^{13}C than C_4 plants resulting in lighter $\delta^{13}C$ signatures by on average ∼15‰ (Cerling & Harris, 1999). In Northwest Africa, the landscape is dominated primarily by C_4 grasses and C_3 woody trees and shrubs, allowing for quantitative estimates of woody versus grassy cover using the $\delta^{13}C_{wax}$ method (Garcin et al., 2014). There are few records with adequate resolution to resolve astronomical-scale shifts in monsoon strength and vegetation composition in Northwest Africa since the Pliocene: 5.0–4.6 Ma (Kuechler et al., 2018), 3.6–3.0 Ma (Kuechler et al., 2018), 0.52–0.36 Ma (O'Mara et al., 2022), and 0.13–0 Ma (Kuechler et al., 2013). While discontinuous, these records document a marked decline in the mean state of the monsoon and an increase in C_4 grass cover sometime between ca. 3.0 and 0.5 Ma which are part of longer-term trends of increasing continental aridity and C_4 grass abundance in Northwest Africa since the late Miocene (Crocker et al., 2022). Here we generate new astronomically resolved records of Northwest African monsoon strength, landscape C_3/C_4 balance, dust flux, and opal flux from 1.1 to 1.0 Ma to add new timing constraints and assess various potential mechanisms impacting environmental shifts in Northwest African climate and ecology during the Plio-Pleistocene.

3. Materials and Methods

3.1. Marine Core Sites

Marine sediment core MD03-2705 (18°05′N, 21°09′W) was taken aboard the RV Marion Dufresne along the submarine ridge that connects the Mauritanian coast to the Cape Verde Islands at a water depth of 3,085 m below sea level (Jullien et al., 2007). The core site is located at the apex of a 300 m seamount and is ∼500 km offshore which severely limits the potential inputs of riverine sediments or major alterations by turbidites or contourites. The 37-m-long core spans the last 1.1 Myrs. The age-depth model was determined by peak-to-peak matching of $\delta^{18}O$ measurements of benthic foraminifera (Malaizé et al., 2012) with the astronomically tuned LR04 benthic stack (Lisiecki & Raymo, 2005) and was previously published in O'Mara et al. (2022).

In this work, plant-wax concentration and isotope samples (n = 23) and $^3He_{ET}$-normalized dust, opal, and carbonate fluxes (n = 24) were measured every 10 cm (∼4 kyr intervals) between 1.1 and 1.0 Ma to capture astronomical-scale variability during the MPT. These new data are compared with previously published estimates from MD03-2705 (O'Mara et al., 2022; Skonieczny et al., 2019) and ODP site 659 (Kuechler et al., 2013, 2018). ODP 659 (18°04.6′N, 21°01.57′W, 3,070 mbsl) is within 13 km of MD03-2705 and is assumed to have equivalent sources of sedimentary material.

3.2. Organic Biomarker Analysis

Plant-wax *n*-alkanes were extracted from freeze-dried and homogenized sediment samples using an accelerated solvent extractor. *N*-alkanes were further isolated and purified using silica gel column chromatography and urea

adduction before quantification using gas chromatography mass spectrometry (see Supporting Information S1 for detailed procedures). Compound specific $\delta^{13}C$ and δD measurements were made on *n*-alkanes (chain lengths C_{25}–C_{35}) using gas chromatography isotope ratio mass spectrometry. *N*-alkanes were combusted (pyrolyzed) to CO_2 (H_2) gas for carbon (hydrogen) isotope measurements. $\delta^{13}C$ and δD values were converted to ‰VPDB and ‰VSMOW scales based on repeated measurements of external authentic standards of known isotope ratios interspersed throughout sample runs. Uncertainty was calculated following Polissar and D'Andrea (2014). Across C_{27}–C_{33} *n*-alkane homologs, mean estimated 1σ errors were 0.14‰ for carbon and 4.31‰ for hydrogen.

Two steps are applied to calculate δD_{Precip} from δD_{wax}. First, the biosynthetic fractionation of hydrogen during wax formation is estimated using the fraction of C_3 trees versus C_4 grasses which produced the *n*-alkanes. This is calculated using a two endmember $\delta^{13}C$ mixing model (see Supporting Information S1). Second, the change in the hydrogen isotope composition of sea water which varies as a function of global ice volume change was corrected for using changes in the LR04 benthic isotope stack (Lisiecki & Raymo, 2005). The last-glacial maximum benthic foraminifera $\delta^{18}O$ was scaled with the known change in sea water $\delta^{18}O$ composition of 1‰ since the last glacial maximum (Schrag et al., 2002) and converted to changes in δD using the global meteoric water relationship of $\delta^{18}O$:δD of 1:8. This correction is small (mean = 3.3‰) compared to the variability present in the record (~20–30‰).

No corrections were applied to the $\delta^{13}C_{wax}$ measurements. Variability in the $\delta^{13}C$ of CO_2 in the atmosphere ($\delta^{13}C_{CO2}$) can potentially lead to biases in the carbon isotopic composition of plant waxes, but these are likely to be very small and are not systematically predictable. See Supporting Information S1 for further discussion.

3.3. Dust and Biogenic Opal Flux Analysis

3.3.1. Sedimentology

Sediment deposition at MD03-2705 site is dominated by biogenic calcium carbonate, silt and clay particles, biogenic opal, and very small amounts of organic carbon (Jullien et al., 2007; Skonieczny et al., 2019). $CaCO_3$ percentages were calculated using coulometry and biogenic opal percentages were determined using alkaline extraction and molybdate blue spectrophotometry following Mortlock and Froelich (1989). Because the detrital material deposited at MD03-2705 site is essentially entirely aeolian in origin (Skonieczny et al., 2019), dust percentages were calculated by subtracting the $CaCO_3$ and biogenic opal mass fractions from one:

$$F_{dust} = 1 - F_{CaCO_3} - F_{opal} \tag{1}$$

3.3.2. Helium Isotopes and Constant Flux Normalization

Fluxes were determined using the extraterrestrial ^3He ($^3He_{ET}$) normalization technique (Farley, 2001; Marcantonio et al., 1996) which calculates instantaneous fluxes for each sample (Costa et al., 2020; McGee & Mukhopadhyay, 2013). Sediment helium isotopic compositions ($^3He/^4He$) were measured in carbonate-free, freeze-dried sediment samples on a MAP-215 mass spectrometer following the procedure of Winckler et al. (2005).

The helium isotopic composition of marine sediments represents a mixture of terrestrial dust and extraterrestrial interplanetary dust particles (IDPs). IDPs have ^3He concentrations orders of magnitude higher than terrestrial material (Nier & Schlutter, 1992). Measured ^3He concentrations were converted to extraterrestrial concentrations ($^3He_{ET}$) using a binary mixing model using an IDP end member $^3He/^4He$ ratio of 2.4×10^{-4} (Nier & Schlutter, 1992) and a terrestrial end member for North Africa of 1×10^{-8} as described by (O'Mara et al., 2022):

$$\left[{}^3He_{ET}\right]\left(\text{pcc g}^{-1}\right) = \left[{}^3He_{meas}\right]\left(\text{pcc g}^{-1}\right) * \left\{\frac{1 - \frac{{}^3He/{}^4He_{Terr}}{{}^3He/{}^4He_{meas}}}{1 - \frac{{}^3He/{}^4He_{Terr}}{{}^3He/{}^4He_{IDP}}}\right\} \tag{2}$$

Mass accumulation rates (MAR) were then calculated by diving the flux of $^3He_{ET}$ from space ($^3He_{IDP}$ flux = 0.8 pcc cm^{-2} kyr^{-1}) (McGee & Mukhopadhyay, 2013) by the measured $^3He_{ET}$ concentration in each sample.

$$\text{MAR}\left(\text{g cm}^{-2}\ \text{kyr}^{-1}\right) = {}^{3}\text{He}_{\text{IDP}}\ \text{flux}\left(\text{pcc cm}^{-2}\ \text{kyr}^{-1}\right)\ \left[{}^{3}\text{He}_{\text{ET}}\left(\text{pcc g}^{-1}\right)\right. \quad (3)$$

Dust and opal fluxes were calculated by multiplying their mass fraction by the MAR. Uncertainties were determined via error propagation of analytical error on ^{3}He and ^{4}He concentration measurements (air standard He concentration uncertainty $1\sigma = 1\%$), replicate concentration fractional differences (^{3}He $1\sigma = 42\%$, ^{4}He $1\sigma = 37\%$), a nominal 5% uncertainty for mass fraction estimates, and a $1\sigma = 40\%$ uncertainty in the IDP $^3\text{He}_{\text{ET}}$ flux (McGee & Mukhopadhyay, 2013).

3.4. Atmospheric CO_2 Estimates

We compare our vegetation records to atmospheric CO_2 levels because they affect the competitive interactions between savanna C_4 grasses versus C_3 trees. Direct measurements of atmospheric CO_2 concentrations from ice cores extend back only to ca. 800 ka (Lüthi et al., 2008). A recently published approach leveraging the strong impacts of atmospheric pCO_2 on landscape C_3/C_4 vegetation balance in Northeastern India—as recorded by the high correlation between $\delta^{13}C$ of plant-wax fatty *n*-acids (FA) preserved in Bay of Bengal sediments and atmospheric pCO_2 over the last 800 kyr—has extended continuous, high-resolution estimates of pCO_2 back to 1.46 Ma (Yamamoto et al., 2022). However, during our study interval (1.1–1.0 Ma) this new CO_2^{FA} record lacks CO_2 estimates between 1.048 and 1.030 Ma missing nearly an entire precession cycle, hampering our astronomical time-scale analysis. In contrast, the LR04 benthic stack (Lisiecki & Raymo, 2005), which is highly correlated with atmospheric CO_2 concentrations, is resolved at 2 kyr resolution during our study interval. For this reason, here we opt to leverage the LR04 $\delta^{18}O$ versus EPICA pCO_2 relationship to generate an estimated time series of atmospheric CO_2 concentration to compare with our MPT $\delta^{13}C_{\text{wax}}$ record (See Supporting Information S1 for details). We compare our new vegetation record with estimated atmospheric pCO_2 during the MPT to assess the impact of changing CO_2 levels on Northwest African ecosystem composition.

3.5. Statistical Analysis

All linear regressions were calculated by first interpolating the higher resolution record to the time scale of the lower resolution record. Correlation coefficients were calculated using the MATLAB (v. 2021b) command "fitlm" and corresponding *p*-values that take into account autocorrelation between the two time series were calculated following Ebisuzaki (1997). All multivariate linear regressions were also calculated in MATLAB using the "regress" command. Insolation and astronomical parameter time series were generated using the MATLAB package "daily_insolation" (Eisenman & Huybers, 2006) following astronomical solutions from Berger (1978) and Berger and Loutre (1991). Two sample Kolmogorov-Smirnov tests (KS test) were performed using the MATLAB command "kstest2."

4. Results

4.1. Plant-Wax *n*-Alkane Concentrations and Distributions

The long chain C_{25}–C_{35} *n*-alkanes represent a dominantly terrestrial plant source. Sedimentary *n*-alkane concentrations are dominated by long chain-length homologs (C_{25}–C_{35}) ranging from 2.98 to 12.24 μg g^{-1} dry sediment (average 6.34). Medium chain length homologs (C_{16}–C_{22}) are also present in significant quantities (0.37–10.94, average 4.99 μg g^{-1} dry sediment) indicating contributions from algal and/or moss sources (Baas et al., 2000; Bush & McInerney, 2013; Ficken et al., 2000; Nott et al., 2000). However, high carbon preference index values of 5.36–7.53 (average 6.51) for the long chain C_{25}–C_{35} *n*-alkanes confirm these homologs are from a terrestrial plant source (Bush & McInerney, 2013; Eglinton & Hamilton, 1967). CPI was uncorrelated with any of the proxy or forcing variables considered in this study. The average chain lengths of the C_{25}–C_{35} alkanes exhibit a tight range from 29.87 to 30.16 (average 30.41). The C_{31} homolog is the most abundant in all samples, as is typical for modern African vegetation (Garcin et al., 2014).

4.2. Carbon Isotopic Composition of *n*-Alkanes

The carbon isotopic composition of the C_{27}–C_{33} *n*-alkanes show similar patterns over the study interval: $R_{27/29} = 0.72$, $R_{27/31} = 0.75$, $R_{27/33} = 0.55$, $R_{29/31} = 0.86$, $R_{29/33} = 0.61$, $R_{31/33} = 0.77$. We therefore limit the following discussion to the C_{31} *n*-alkane record (hereafter $\delta^{13}C_{\text{wax}}$) as it is the most abundant of the long chain *n*-alkanes in

our samples and is generally the most abundant homolog in African vegetation (Bush & McInerney, 2013; Garcin et al., 2014; Polissar et al., 2021). We opted to avoid using a $\delta^{13}C_{wax}$ weighted average approach due to the potential compounding environmental factors such as temperature (Bush & McInerney, 2015) and aridity (Vogts et al., 2012) on alkane chain length distributions, which could obfuscate the landscape-scale vegetation composition estimates sought here using the $\delta^{13}C_{wax}$ proxy. This decision however does not impact the conclusions of the present study as $\delta^{13}C_{31}$ is highly correlated with concentration weighted $\delta^{13}C_{wax}$ estimates across C_{27} to C_{33} homologs ($r^2 = 0.93$, $p < 0.001$). The range of $\delta^{13}C_{wax}$ values spans −24.9 to −23.4‰ VPDB (average −24.1‰). Using a linear mixing model between end member values of C_4 grasses ($\delta^{13}C_{C4} = -19.9‰$) and C_3 trees ($\delta^{13}C_{C3} = -33.6‰$) in Africa estimated from a compilation of previous studies (Badewien et al., 2015; Bezabih et al., 2011; Garcin et al., 2014; Kristen et al., 2010; Magill et al., 2013), these $\delta^{13}C_{wax}$ signatures imply a range of C_4 plants in the *n*-alkane source region of 64%–75% (average 70%). This is consistent with modern West African terrestrial environments dominated by C_4 grasslands and mixed C_4 grassy/C_3 woody savannas, within which C_4 grasses typically represent 60%–100% of vegetation cover (Sankaran et al., 2005; Staver et al., 2011) and ∼72% of net primary productivity (Lloyd et al., 2008).

4.3. Hydrogen Isotopic Composition of *n*-Alkanes

As with the $\delta^{13}C$ values of our *n*-alkane records, the hydrogen isotopic composition of the C_{27}–C_{33} *n*-alkane homologs show nearly identical patterns through time and are highly positively correlated: (R ranges from 0.82 to 0.95). Likewise, δD_{Precip} values (corrected for changes in vegetation and global ice volume) estimated from each homolog are similarly correlated. We restrict the remainder of the discussion to the estimated hydrogen isotopic composition of precipitation from the C_{31} *n*-alkane (hereafter δD_{Precip}). Estimates of δD_{Precip} range from −52.9 to −8.1‰ VSMOW (average −32.7‰).

4.4. Dust and Opal Fluxes

Downcore dust percentages range from 21.4% to 86.4% (average 35.8%) and dust fluxes range from 0.69 to 3.15 g cm^{-2} kyr^{-1} (average 1.54 g cm^{-2} kyr^{-1}). Opal percentages and fluxes are substantially lower ranging from 1.3% to 8.2% (average 2.5%) and 0.04–0.22 g cm^{-2} kyr^{-1} (average 0.10 g cm^{-2} kyr^{-1}). Both dust versus opal percent and flux are linearly correlated with each other ($R_{\%dust/opal} = 0.83$ and $R_{Fdust/opal} = 0.79$).

5. Discussion

5.1. Astronomical Scale Hydroclimate, Vegetation, Dust, and Opal Variability

Monsoon strength, landscape C_3/C_4 plant balance, dust flux, and marine productivity exhibit strikingly similar evolutions between 1.1 and 1.0 Ma (Figure 2). All four proxy records are characterized by four cycles, which correlate with swings in local insolation and the summer inter-hemispheric insolation gradient (Table S1 in Supporting Information S1), both of which have been shown to be important drivers of monsoon strength later in the Pleistocene (O'Mara et al., 2022) and in the Pliocene (Kuechler et al., 2018). These new plant-wax derived estimates of δD_{Precip} are consistent with the hypothesis that the tempo and amplitude of wet/dry cycles in Northwest Africa have been continuously set by low-latitude insolation forcings at least as far back as the Miocene (Crocker et al., 2022). During wet monsoon intervals, grasslands expand into the Sahara resulting in more positive $\delta^{13}C_{wax}$ values (Kuechler et al., 2013). Concurrently, dust fluxes are reduced as trade wind (Harmattan wind) influence is minimized, soil moisture is higher, and expanded vegetation cover restricts dust entrainment into the atmosphere. Opal fluxes are also lower during wet monsoon intervals. Opal flux in West African margin sediments during the last ca. 20 kyr show that decreases (increases) in paleo-productivity are tightly linked with decreases (increases) in trade wind strength and dust fluxes on millennial timescales (Bradtmiller et al., 2016). Here we show that this relationship between Saharan dust flux and eastern North Atlantic marine productivity holds on astronomical timescales and across the MPT.

5.2. Variable Effects of Rainfall and CO_2 on Landscape-Scale C_3/C_4 Balance Reveal Ecosystem Range Shifts

The regional balance of C_3 trees versus C_4 grasses in Northwest Africa during the late-Pleistocene are sensitive to both changes in monsoon strength and atmospheric CO_2 levels (O'Mara et al., 2022). However, no relationship between estimated atmospheric CO_2 concentrations and $\delta^{13}C_{wax}$ exists in our new MPT record (Figures 2f and

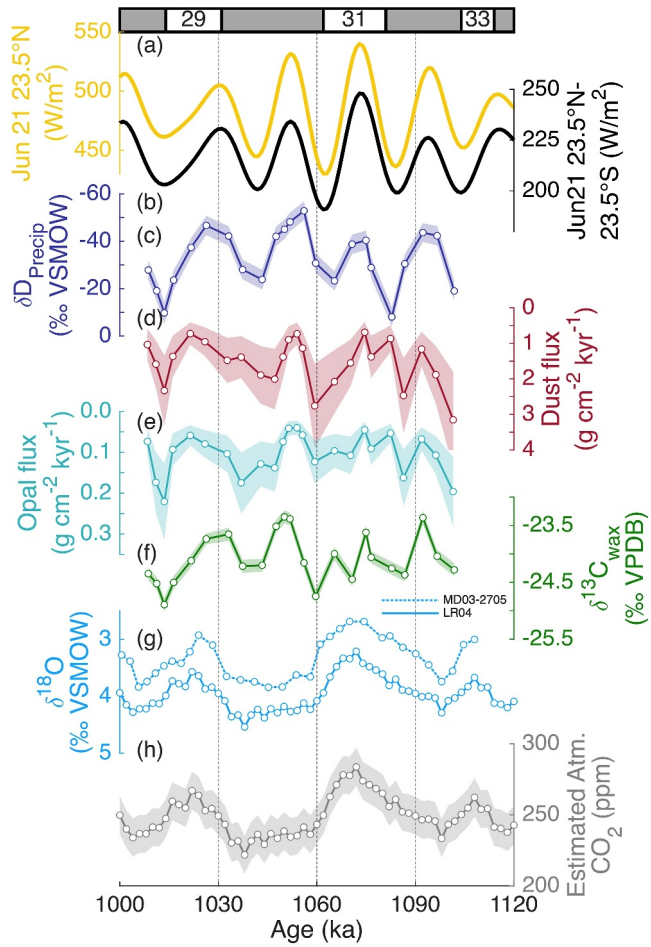

Figure 2. New records of plant-wax carbon and hydrogen isotopes and dust and opal flux from MD03-2705 compared with potential forcings. (a) Local summer insolation (23.5°N, June 21). (b) Summer inter-hemispheric insolation gradient (23.5°N–23.5°S, June 21). (c) Plant wax-derived precipitation hydrogen isotopes. (d) $^{3}He_{ET}$-normalized dust flux. (e) $^{3}He_{ET}$-normalized opal flux. (f) *n*-C_{31} $\delta^{13}C_{wax}$ ($\Delta 1‰ \approx \Delta 7.3\%$ C_4). (g) Benthic foram $\delta^{18}O$ from MD03-2705 (dashed line) (Malaizé et al., 2012) and the global benthic $\delta^{18}O$ stack (solid line) (Lisiecki & Raymo, 2005). (h) Estimated atmospheric CO_2 concentrations (method described in Text S5 in Supporting Information S1) using the global benthic $\delta^{18}O$ stack (solid line) (Lisiecki & Raymo, 2005), and ice core CO_2 data from Higgins et al. (2015) and Lüthi et al. (2008). Shading in (c)–(f), and (h) indicates estimated 1σ uncertainty. Marine isotope stage boundaries are indicated at the top of the figure.

2h). During 0.13–0 and 0.52–0.36 Ma, increases in monsoon rainfall (δD_{Precip}) were accompanied by increased $\delta^{13}C_{wax}$ values consistent with northward expansions of C_4 grasslands into the Sahara. Additionally, increased atmospheric CO_2 concentrations co-occurred with more negative $\delta^{13}C_{wax}$ values suggesting that higher CO_2 facilitated increased C_3 tree cover in savannas (O'Mara et al., 2022). Surprisingly, we find no relationship between estimated atmospheric CO_2 concentrations and $\delta^{13}C_{wax}$ ($p = 0.72$) during 1.1–1.0 Ma. This difference likely reflects a shift in the distribution of grassland and savanna ecosystems between these time slices. Decreased sourcing of savanna plant-waxes to the core site would reduce the strength of any CO_2 signal because CO_2 will influence C_3/C_4 balance in savannas but will not have an impact on grasslands which are perennially dominated by C_4 vegetation.

The $\delta^{13}C_{wax}$ values recorded in our core site (MD03-2705) record an integrated signal of dynamic landscape changes across multiple ecosystems where the effects of rainfall, CO_2, and disturbance on net landscape C_3/C_4 balance vary. When ecosystem ranges are located at far southerly positions, the plant waxes supplied to our core site will be sourced in a greater proportion from the moisture limited grasslands along the southern edge of the Sahara and the $\delta^{13}C_{wax}$ record will be more sensitive to changes in rainfall (δD_{Precip} vs. $\delta^{13}C_{wax}$ will have a negative slope; wetter conditions lead to more C_4 grassy vegetation). Rainfall will have a similar, but opposite impact on the $\delta^{13}C_{wax}$ record when ecosystems are situated at far northerly positions. In this situation the wax source will have a greater proportion of forests opposed to grasslands, so increased rainfall will cause tropical forest expansion (δD_{Precip} vs. $\delta^{13}C_{wax}$ will have a positive slope; wetter conditions lead to more C_3 woody vegetation). However, when ecosystems are located at positions intermediate to these two extremes, the wax source area is dominated by mixed woody/grassy savanna vegetation and thus the $\delta^{13}C_{wax}$ record will exhibit a greater sensitivity to ecosystem C_3/C_4 balance resulting from changes in atmospheric CO_2. Because the West African margin is geologically passive, the positions of the core sites of MD03-2705 and ODP 659 have remained constant relative to the African continent over the last few million years while these ecosystem boundaries varied substantially (Dupont, 1993; Leroy & Dupont, 1994). We can therefore use the relative effects of rainfall and CO_2 on regional C_3/C_4 balance as a means of estimating the paleopositions of these grassland versus savanna versus forest ecosystems: strong hydrologic influence indicates extreme positions of ecosystem boundaries (north vs. south distinguished by the rainfall vs. C_3/C_4 slope) while a stronger CO_2 influence compared to rainfall indicates more intermediately situated ecosystem boundaries.

Variable relationships between hydroclimate, landscape vegetation composition, and atmospheric CO_2 show a broadly equatorward contraction of ecosystem ranges over the last 5 Myr with large fluctuations during the late-Pleistocene. During the mid-Pliocene Warm Period (mPWP; 3.3–3.0 Ma) (Dowsett et al., 2010; Haywood et al., 2010) ecosystems were in their farthest northward position (Figures 3a–3d). Plant wax data from Kuechler et al. (2018) show that δD_{Precip} and $\delta^{13}C_{wax}$ are positively correlated ($R = 0.29$, $p < 0.05$) while there is no significant relationship between atmospheric CO_2 and $\delta^{13}C_{wax}$ (Figure 3l). In contrast, ecosystems were positioned at their farthest southward position during 1.1–1.0 Ma (Figures 3a–3d). During 1.1–1.0 Ma we find a strong linear relationship between C_3/C_4 balance ($\delta^{13}C_{wax}$) and monsoon rainfall (δD_{Precip}) ($R = -0.68$, $p < 0.001$) but no clear relationship between $\delta^{13}C_{wax}$ and estimates of atmospheric CO_2 concentrations ($R = -0.13$, $p = 0.72$) (Figure 3k). During 0.52–0.36 Ma ecosystems were situated at an intermediate northward position; $\delta^{13}C_{wax}$ was highly correlated with atmospheric CO_2 levels ($R = -0.81$, $p = 0.001$) while only weakly related to δD_{Precip} ($R = -0.22$, $p = 0.15$) (Figure 3j). Between 0.13 and

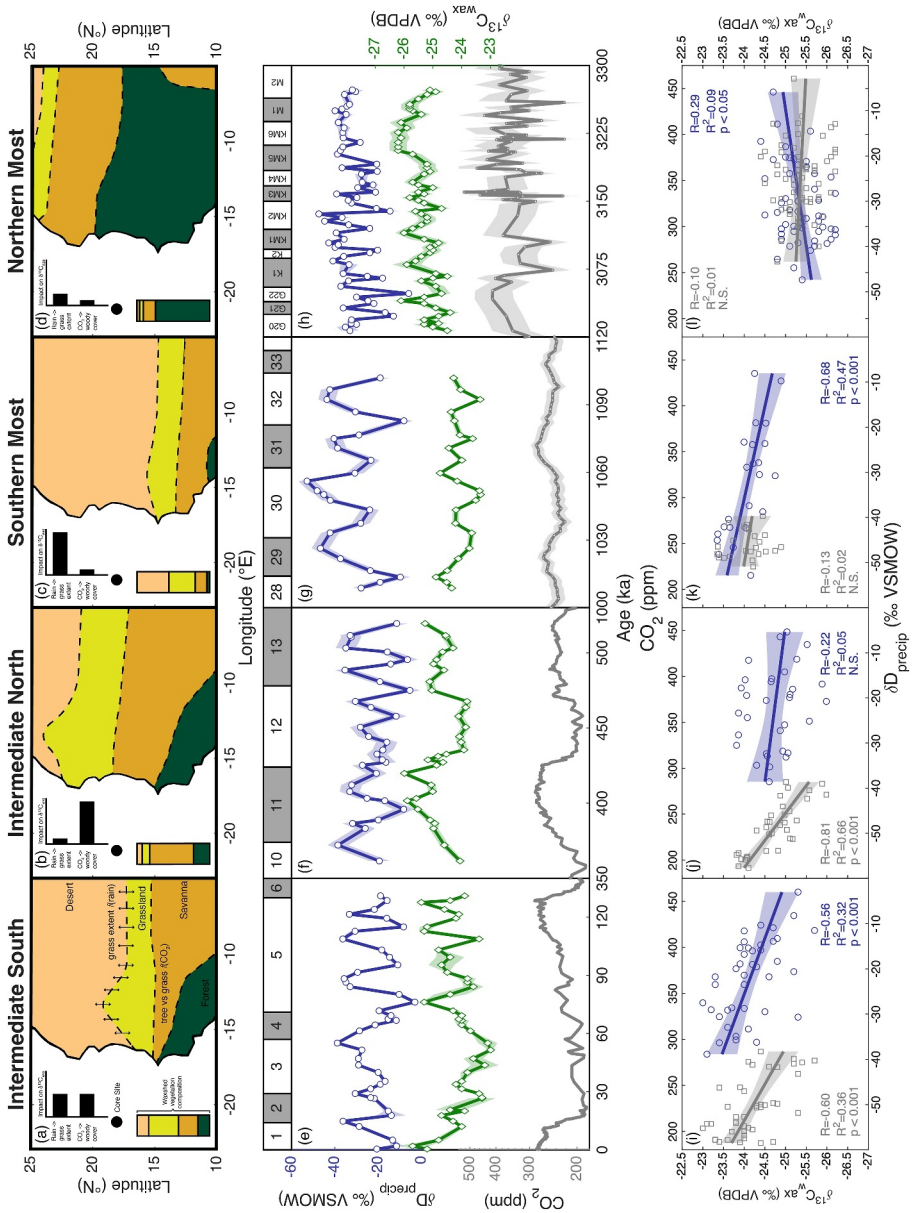

Figure 3. Variable rainfall and CO_2 controls on regional C_3/C_4 balance reveal shifting ecosystem distributions. (a–d) Conceptual diagrams demonstrating how the northward extent of ecosystems impact the $\delta^{13}C_{wax}$ recorded at ODP 659 (a, d) and MD03-2705 (b, c). Vegetation boundaries represent approximate mean locations for intervals based on marine pollen records (Hooghiemstra et al., 2006) (a), (Dupont, 1993) (b), and model simulations (Salzmann et al., 2008) (d) While no pollen or model evidence provide direct constraints for boundaries in (c). Boundaries between ecosystems will vary with astronomical forcing. (e) δD_{Precip} (blue) and $\delta^{13}C_{wax}$ (green) from Kuechler et al. (2013), CO_2 (gray) from Lüthi et al. (2008). Note that $\Delta 1‰$ $\delta^{13}C_{wax} \approx \Delta 7.3\%$ C_4. (f) δD_{Precip} (blue) and $\delta^{13}C_{wax}$ (green) from O'Mara et al. (2022), CO_2 (gray) from Lüthi et al. (2008). (g) δD_{Precip} (blue) and $\delta^{13}C_{wax}$ (green) from (this study), estimated CO_2 (gray, this study, see Text S5 in Supporting Information S1 for calculation). (h) δD_{Precip} (blue) and $\delta^{13}C_{wax}$ (green) from Kuechler et al. (2013), estimated CO_2 from $\delta^{11}B$ paleo-barometer (De La Vega et al., 2020; Dyez et al., 2018; Martínez-Botí et al., 2015; Sosdian et al., 2018) compiled and vetted by Cenozoic CO2 Proxy Integration Project (CenCO2PIP) Consortium et al. (2023). (i) Linear regression (LR) of δD_{Precip} versus $\delta^{13}C_{wax}$ ($R = -0.56$, $p < 0.001$) and CO_2 versus $\delta^{13}C_{wax}$ ($R = -0.60$, $p = 0.015$); multivariate linear regression (MLR) of δD_{Precip} and CO_2 versus $\delta^{13}C_{wax}$ ($r^2 = 0.59$, $p < 0.001$) (not shown) from data in panel (e). (j) LR of δD_{Precip} versus $\delta^{13}C_{wax}$ ($R = -0.22$, $p = 0.15$) and CO_2 versus $\delta^{13}C_{wax}$ ($R = -0.81$, $p = 0.001$); MLR of δD_{Precip} and CO_2 versus $\delta^{13}C_{wax}$ ($r^2 = 0.80$, $p < 0.001$) (not shown) from data in panel (f). (k) LR of δD_{Precip} versus $\delta^{13}C_{wax}$ ($R = -0.68$, $p < 0.001$) and CO_2 versus $\delta^{13}C_{wax}$ ($R = -0.13$, $p = 0.72$); MLR of δD_{Precip} and CO_2 versus $\delta^{13}C_{wax}$ ($r^2 = 0.47$, $p = 0.002$) (not shown) from data in panel (g). (l) LR of δD_{Precip} versus $\delta^{13}C_{wax}$ ($R = 0.29$, $p = 0.02$) and CO_2 versus $\delta^{13}C_{wax}$ ($R = -0.1$, $p = 0.45$); MLR of δD_{Precip} and CO_2 versus $\delta^{13}C_{wax}$ ($r^2 = 0.11$, $p = 0.03$) (not shown) from data in panel (g) Shading about time series indicate 1σ uncertainty. Marine isotope stage boundaries (Lisiecki & Raymo, 2005) are shown above time series panels.

0 Ma, ecosystems were situated at an intermediate southward position. During this period, CO_2 concentrations and δD_{Precip} are similarly related to $\delta^{13}C_{wax}$ ($R = -0.60$, $p = 0.015$; $R = -0.56$, $p < 0.001$, respectively) explaining similar amounts of the variance in the $\delta^{13}C_{wax}$ record ($r^2 = 0.36$, $r^2 = 0.32$) (Figure 3i). Together, these data suggest that during these four intervals, desert/grassland and savanna/forest ecosystem boundaries were at their northernmost position during the mPWP, contacted to their southernmost position during 1.1–1.0 Ma, rebounded to an intermediate northerly position during 0.52–0.36 Ma before retreating to an intermediate southerly location during 0.13–0 Ma (Figures 3a–3d).

We note that lower glacial-interglacial CO_2 variability during the MPT cannot explain the largely absent vegetation response to atmospheric CO_2 swings. Excluding the post-industrial period, atmospheric CO_2 levels over the last 500 kyr have varied between 184 and 299 ppm (115 ppm range) while during 1.1–1.0 Ma the range was much smaller (206–269 ppm, range 63 ppm). If the sensitivity of the ecosystem C_3/C_4 balance to CO_2 concentrations was similar during the MPT compared to the last 500 years, we would still expect to observe glacial-interglacial swings in $\delta^{13}C_{wax}$ on the order of 1‰. Such glacial-interglacial variability is not present at all in the new $\delta^{13}C_{wax}$ record. The consistent timing (within ∼1–2 kyr) between swings in atmospheric CO_2 and $\delta^{13}C_{wax}$ observed previously (O'Mara et al., 2022) demonstrates a fairly rapid ecosystem response to CO_2 forcing. We would therefore still expect to observe such a response despite the shorter duration of glacial periods during the 1.1–1.0 Ma time slice. We thus interpret this strong coupling between increased monsoon rainfall and expanded C_4 grasslands, with a simultaneous lack of CO_2 forcing during 1.1–1.0 Ma as evidence of southwardly shifted ecosystem boundaries during this time. The shift from more northerly ecosystem boundaries toward more southerly boundaries between 0.52–0.36 and 0.13–0 Ma is corroborated by terrestrial ecosystem reconstructions of the desert/savanna and savanna/forest boundary paleo-latitudes from a transect of marine core-based pollen reconstructions, which show the savanna/desert and forest/savanna boundaries were on average 1.6° and 1.3° farther northward respectively between 0.52 and 0.36 compared to 0.13–0 Ma (Dupont, 1993) (Figure 6c). Direct pollen reconstructions of ecosystem boundary paleo-latitudes, which require a transect of multiple pollen records along the Northwest African margin, do not exist for time periods earlier than 0.7 Ma. However, the northerly ecosystem ranges during the Pliocene are evidenced by pollen records from two sites off Northwest Africa, ODP 658 (Leroy & Dupont, 1994) and ODP 659 (Vallé et al., 2014), as well as vegetation model simulations (Salzmann et al., 2008).

5.3. Plio-Pleistocene Evolution and Potential Drivers of the North African Hydroclimate and Dust Trends

5.3.1. Northwest African Hydroclimate

Our new MPT record and the other δD_{Precip} records presented here are consistent with a dominantly astronomical control (via precession and obliquity-paced changes in low-latitude insolation) on Northwest African monsoon rainfall variability since at least 5 Ma (Kuechler et al., 2013, 2018; O'Mara et al., 2022). Yet monsoon strength declined by ∼30% sometime between 1.0 and 0.52 Ma despite no secular change in these insolation forcings. Using the data currently available, below we test several proposed mechanisms for what is driving the observed Northwest African monsoon decline between 1.0 and 0.5 Ma. A definitive driver is not identified. However, the coincident timing of strengthening North Atlantic SST gradients as well as declining AMOC strength during the MPT with monsoon intensity decline in Northwest Africa provides circumstantial evidence that this aridification may have been the result of changes in atmospheric circulation related to reorganizations of North Atlantic Ocean-atmosphere processes during the MPT.

Using the discontinuous records of δD_{Precip} as benchmarks for changes in monsoon rainfall amount, we test various hypotheses of the potential long-term drivers of Northwest African monsoon strength by statistically comparing the trends in potential forcings with the δD_{Precip} data from the two Pliocene and three Pleistocene time slices. While the summer inter-hemispheric insolation gradient sets the tempo and amplitude of monsoon variability, we show here that the stationary mean of astronomical variability across the Plio-Pleistocene cannot explain the mid- to late-Pleistocene monsoon decline. Two sample KS tests reveal that insolation forcing was statistically indistinguishable in each time slice (Figures 4e and 4k). The onset of a stronger east-west sea surface temperature (SST) gradient in the equatorial Pacific, establishing the modern Walker circulation during the early Pleistocene is thought to have caused drying in Central Africa (Ravelo et al., 2004). However, this shift occurs ∼1 Myr too early to explain the reduction in Northwest African monsoon strength (Figure 4f) (Brierley & Fedorov, 2010; Ravelo et al., 2004). Cooler tropical sea surface temperatures could result in decreased

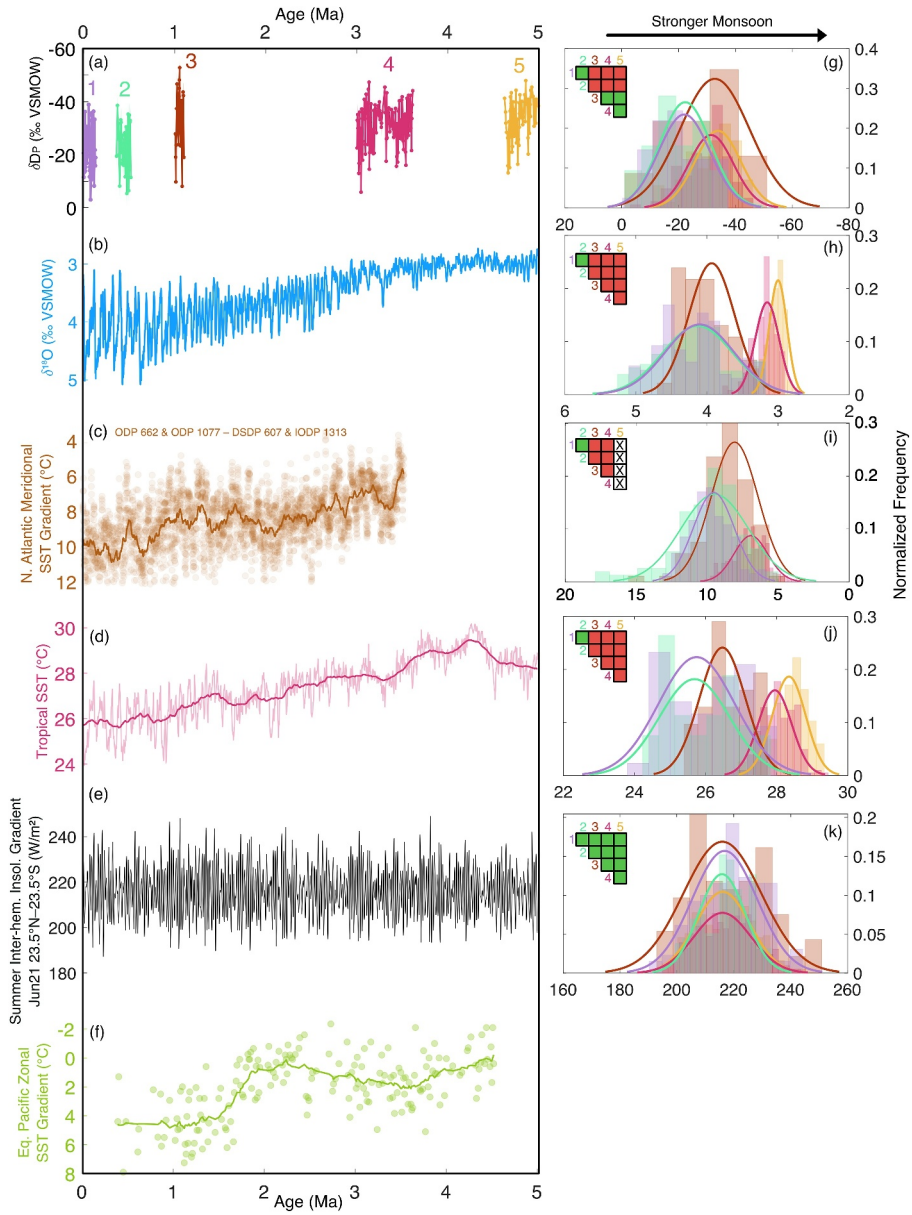

Figure 4. Analysis of MPT monsoon shift forcing. (a) δD_{Precip} from Kuechler et al. (2013, 2018) and O'Mara et al. (2022) and this study (b) Global benthic $\delta^{18}O$ stack (Lisiecki & Raymo, 2005) (c) Alkenone-based SST gradient between the tropical Atlantic (ODP 662 1°S, 11°W (Herbert et al., 2010) and ODP 1077 11°S, 10°E (Schefuß et al., 2003)) and the mid-latitude North Atlantic (DSDP 607 (Lawrence et al., 2010) and IODP 1313 (Naafs et al., 2010, 2012)). (d) Alkenone-derived tropical SST stack (Herbert et al., 2010). (e) Summer inter-hemispheric insolation gradient (23.5°N–23.5°S, June 21). (f) Mg/Ca-derived tropical Pacific zonal SST gradient (ODP 806–ODP 847) data originally from Wara et al. (2005) and recalculated based on updated Mg/Ca_{SW} by O'Brien et al. (2014). (g–k) Normalized histograms with Gaussian fits for the δD_{Precip} proxy (g) and analogous time intervals for each forcing (h–k). The units of the *x*-axes correspond to *y*-axis of the adjacent panel. Inset grid shows the results of two sample Kolmogorov-Smirnov tests: green indicates statistically indistinguishable distributions, while red indicates statistically different distributions ($\alpha = 1\%$).

evaporation over the ocean and a reduced land-sea thermal contrast, both of which have the potential to decrease monsoon rainfall (Schefuß et al., 2003). While tropical ocean SSTs are statistically indistinguishable between the late Pleistocene windows (0.52–0.36 Ma and 0.13–0 Ma), the Pliocene through middle Pleistocene windows show progressive cooling rather than a state change at the MPT, different from the monsoon strength trajectory (Figures 4d and 4j). Some climate model simulations predict that more expansive Northern Hemisphere ice sheets result in increased southerly excursions of cool and dry subtropical airmasses into tropical latitudes, potentially

linking increased global ice volume with decreased Northwest African monsoon strength (Chou & Neelin, 2003). Global ice volume exhibits a similar evolution compared to tropical SSTs, also declining from the Pliocene to mid-Pleistocene in the absence of a decline in monsoon strength (Figures 4b and 4h). Climate model simulations also show that stronger meridional SST gradients which developed over the Plio-Pleistocene may have also led to reductions in the intensity of the Northwest African monsoon (Brierley & Fedorov, 2010). Recent insights from the Coupled Model Intercomparison (CMIP) five experiments demonstrate a clear connection between the meridional Tropical to Northern Hemisphere Extratropical SST gradients (North Atlantic and Mediterranean Sea) and Sahel rainfall (Park et al., 2015, 2016). Weakened SST gradients expected in the future under enhanced high-latitude warming relative to the tropics was observed in the models to both increase the strength of the TEJ and shift the AEJ northward, which in conjunction caused enhanced rainfall over North Africa (Park et al., 2015). The available SST data from the mid-latitude North Atlantic over the last 5 Ma show an increase in the meridional SST gradient between the Tropical and Extratropical Atlantic since the Pliocene (though no SST data exist from the earliest Pliocene time slice) (Figure 4c). Although KS tests show a statistically significant increase in the SST gradient between 3.6–3.0 Ma and 1.1–1.0 Ma without a corresponding decline in monsoon strength (Figures 4g and 4i) the particularly stark contrast between the SST gradient pre and post 1.0 Ma is consistent with the shift toward drier monsoon conditions between 1.0 and 0.5 Ma. Thus, the decline in Northwest African monsoon strength observed in the δD_{Precip} paleorecords may have been in part due to a combination of a weakening TEJ and southwardly contracting AEJ across the MPT. However, more complete Plio-Pleistocene monsoon records as well as targeted climate model experiments of the North Atlantic SST gradient using Pleistocene background climate conditions are required to robustly test this hypothesized mechanism.

It is also possible that other Atlantic SST gradients or Mediterranean SSTs could serve as important controls on Northwest African monsoon rainfall. Modern observations show that a greater inter-hemispheric pressure gradient between 20°S and 20°N results in faster WAWJ and the AWJ and subsequently higher moisture delivery to the Northwest African monsoon region (Nicholson, 2013). While the astronomically controlled inter-hemispheric insolation gradient has no trend over time (Figure 4e), it is possible that independent changes in cross equatorial SST gradients in the Tropical Atlantic could additionally impact inter-hemispheric pressure gradients and thus monsoon rainfall. However, new long-term SST records from the subtropical North Atlantic are needed to test such a hypothesis.

One final possible driver of Northwest African aridification—not tested with this statistical analysis—is a change in the nature of the Atlantic meridional overturning circulation (AMOC) during the MPT. Results from the Pliocene Model Intercomparison Project Phase 2 (PlioMIP2) indicate that the AMOC was much stronger during the mPWP (3.3–3.0 Ma) compared to the pre-industrial, namely due to reduced low salinity water input to the North Atlantic from the Arctic Ocean (Raymo et al., 1992; Venz & Hodell, 2002; Weiffenbach et al., 2023). On millennial timescales in the late-Pleistocene, reductions in AMOC strength driven by enhanced glacial meltwater discharge into the North Atlantic lead to southward shifts in the ITCZ (McGee et al., 2018) and subsequent drying in North Africa (Castañeda et al., 2009; Menviel et al., 2021; Mulitza et al., 2008; Tjallingii et al., 2008). Low resolution records of AMOC strength derived from the ε_{Nd} proxy show a substantial decline in AMOC strength during the "MPT-AMOC Crisis" between ca. 960–860 ka (Kim et al., 2021; Pena & Goldstein, 2014; Tachikawa et al., 2021; Yehudai et al., 2021), followed by a recovery to pre-MPT AMOC strength during interglacial periods, but greatly reduced AMOC strength during glacials. It is thus plausible that a decline in AMOC and by extension a southward shift in the tropical rainbelt position may partially explain the decline in Northwest African monsoonal rainfall. However, this mechanism does not explain why the dominant frequencies of rainfall variability are persistently in the precession and obliquity bands and not paced by glacial-interglacial changes in AMOC strength. Future studies which employ transient model simulations or high-resolution reconstructions of changes AMOC strength across multiple glacial-interglacial cycles before, during and after the MPT are needed help rectify the seemingly conflicting drivers of rainfall change between astronomical and million-year timescales.

5.3.2. Trends in Hydroclimate and Dustiness Across North Africa

The marked decline in Northwest African monsoon strength between 1.0 and 0.5 Ma may have been part of a broader scale shift toward more arid conditions across wider North Africa since the Pliocene, but the multitude of factors which impact terrigenous records makes drawing broad-scale conclusions difficult. Eastern Mediterranean Sea sediments from ODP site 967 show a doubling of the terrigenous material input (elevated Ti/Al ratio) and an initial small rise in dust fluxes ca. 3.2 Ma (Grant et al., 2022; Larrasoaña et al., 2003) (Figure 5e). Elemental ratios

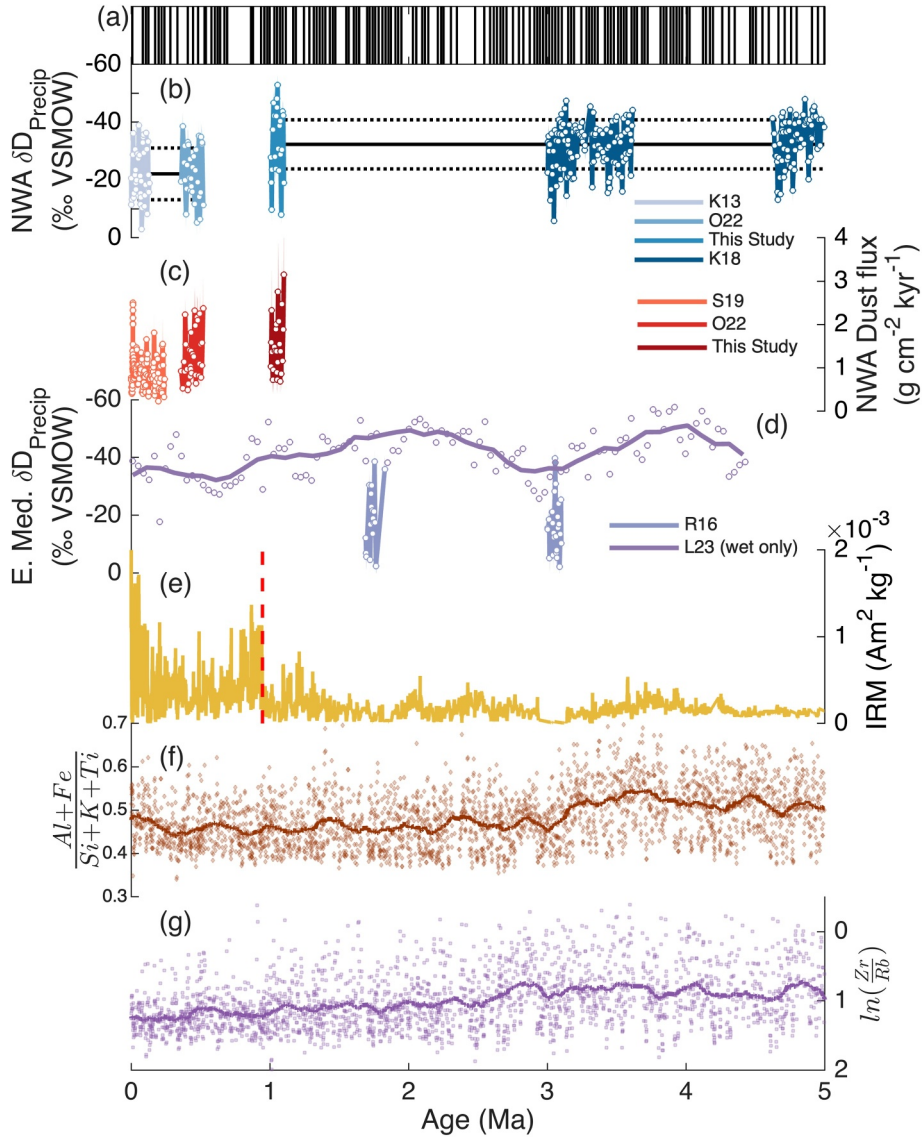

Figure 5. Analysis of MPT monsoon shift forcing. (a) δD_{Precip} from Kuechler et al. (2013, 2018) and O'Mara et al. (2022) and this study (b) Global benthic $\delta^{18}O$ stack (Lisiecki & Raymo, 2005) (c) Alkenone-based SST gradient between the tropical Atlantic (ODP 662 1°S, 11°W (Herbert et al., 2010) and ODP 1077 11°S, 10°E (Schefuß et al., 2003)) and the mid-latitude North Atlantic (DSDP 607 (Lawrence et al., 2010) and IODP 1313 (Naafs et al., 2010, 2012)). (d) Alkenone-derived tropical SST stack (Herbert et al., 2010). (e) Summer inter-hemispheric insolation gradient (23.5°N–23.5°S, June 21). (f) Mg/Ca-derived tropical Pacific zonal SST gradient (ODP 806–ODP 847) data originally from Wara et al. (2005) and recalculated based on updated Mg/Ca_{SW} by O'Brien et al. (2014). (g–k) Normalized histograms with Gaussian fits for the δD_{Precip} proxy (g) and analogous time intervals for each forcing (h–k). The units of the *x*-axes correspond to *y*-axis of the adjacent panel. Inset grid shows the results of two sample Kolmogorov-Smirnov tests: green indicates statistically indistinguishable distributions, while red indicates statistically different distributions ($\alpha = 1\%$).

of [Al + Fe]/[Si + K + Ti] and ln(Zr/Sr) in ODP 659 from the Northwest African margin record a shift from fine grained and more weathered dust delivered to ODP site 659 during the Pliocene transitioning toward coarser grain sizes and less weathered dust beginning ca. 3.1–2.7 Ma reaching a new baseline by 2.25 Ma (Crocker et al., 2022) (Figures 5f and 5g). These data were interpreted to reflect an aridification trend corresponding to the onset of Northern Hemisphere glaciations (Crocker et al., 2022). However, it is possible that the decreased [Al + Fe]/[Si + K + Ti] and increased ln(Zr/Rb) ratios in these same sediments, representing the degree of weathering in dust source regions and dust grain sizes respectively, may have shifted as a result of increased trade winds following the iNHG ca. 2.8 Ma (Vallé et al., 2014) carrying more dust of larger grain sizes from northerly Saharan

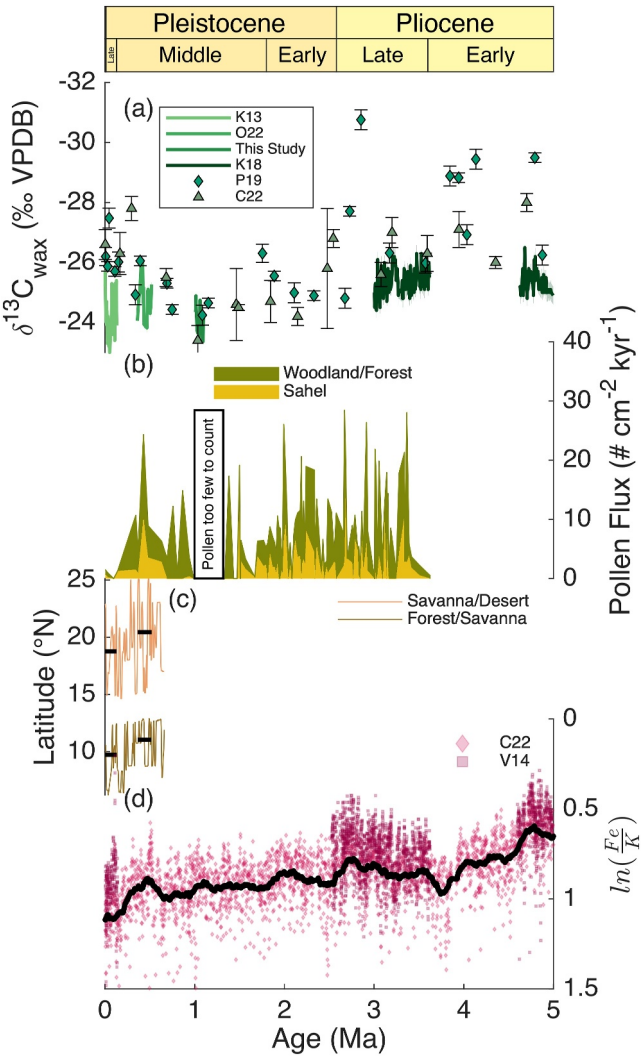

Figure 6. Plio-Pleistocene ecosystem evolution. (a) $\delta^{13}C_{wax}$ from ODP 659 (Crocker et al., 2022; Kuechler et al., 2013, 2018; Polissar et al., 2019) and MD03-2705 (O'Mara et al., 2022, this study). (b) Sahel (yellow) and woodland/forest (green) pollen flux from ODP 659 (Vallé et al., 2014). (c) Paleolatitudes of savanna/desert (orange) and forest/savanna (brown) boundaries in Northwest Africa from Dupont (1993), mean values corresponding to above $\delta^{13}C_{wax}$ time windows are shown in black. (d) XRF-derived estimates of Fe/K elemental ratio from ODP 659 (Crocker et al., 2022; Vallé et al., 2014), black line is 100-point moving average. Geologic epochs from Orndorff et al. (2022) shown above.

(coarser and less weathered) compared to southerly Sahelian (finer and more weathered) sources without the need to invoke a change in regional hydroclimate. Plant-wax δD_{Precip} measurements from ODP 967 exclusively from wet sapropel layers (filtered to remove strong 400- and 1200-kyr eccentricity modulation) indicate declining rainfall intensity during wet monsoon intervals from 4 to 3 Ma, a gradual return to wetter conditions from 3 to 2 Ma, followed finally by drying from 2–present marked by a rapid decline ca. 1 Ma (Lupien et al., 2023) (Figure 5d). However, δD_{Precip} data from this same core which include both wet and dry monsoon conditions show no change in mean value between 1.9–1.6 Ma and 3.1–2.9 Ma (Rose et al., 2016) suggesting the mean state of the monsoon did not vary much over this interval, perhaps due to compensatory drying during weak monsoon intervals (Figure 5d). This lack of mean monsoon strength change is also consistent with recent estimates of steady monsoon runoff to the Eastern Mediterranean from planktic foraminifera $\delta^{18}O$ isotope records also from ODP 967 since 5 Ma (Heslop et al., 2023). A shift toward more negative $\delta^{18}O$ values occurred after 2.6 Ma, but this has been explained by a shift toward more southerly monsoon rainfall source area following iNHG, which is also supported by model simulations (De Boer et al., 2021). Thus, increasing terrigenous material in the Eastern Mediterranean and the Northwest African margin in the late-Pliocene to early Pleistocene was likely due to a combination of factors including regional changes in monsoon rainfall distributions, changes in wind strength, and potentially also declining vegetation cover (see Section 5.4).

A later more dramatic increase in dust flux in the Eastern Mediterranean Sea (ODP site 967) ca. 0.95 Ma occurred coeval with a decrease in the regularity of monsoon-driven sapropel deposits (Figures 5a and 5e) together suggesting greater aridity in North Africa as a whole post 0.95 Ma. The increase in North African aridity inferred from the Eastern Mediterranean records occurred between the wet Northwest African monsoon interval from 1.1 to 1.0 Ma and the drier interval 0.52–0.36 Ma recorded by plant wax-derived estimates of δD_{Precip} (Figure 5b). This correspondence allows for the possibility that West African Monsoon strength may have declined rapidly ca. 0.95 Ma but owing to the various factors other than aridity that can impact dust fluxes, more direct measurements of monsoon rainfall, such as δD_{Precip}, are needed that bridge this gap to test this hypothesis.

In contrast to the eastern Mediterranean, dust fluxes to the Northwest African margin show a modest decline (~13%) between 1.0 and 0.52 Ma (Figure 5c). This decline could be the result of some or all of the factors that influence dust fluxes: available sources, atmospheric entrainment, and transport. The amount of dust available to deflate from the landscape is controlled by the size, soil moisture, vegetation cover, and amount of fine-grained material present in dust source areas (McGee et al., 2010). The speed and positioning of winds then determine the transport potential of dust to a given core site. Multiple records of dust flux to Northwest African margin sediments (Crocker et al., 2022; de Menocal, 1995; Ruddiman et al., 1989; Tiedemann et al., 1994) have shown broadly higher values since the onset of Northern Hemisphere glaciation ca. 2.8 Ma. While initially interpreted to reflect continental aridification such records have been more recently interpreted as likely influenced by increasing wind strength owing to higher pole to equator temperature gradients post-iNHG (Crocker et al., 2022). Dust records (Abell et al., 2021) as well as models (Li et al., 2015) suggest that westerly winds have strengthened and migrated equatorward over this interval. If this were also true for the Northeasterly Harmattan winds, we would expect increasing dust fluxes at our core site. We observe the opposite trend. Similarly, drier conditions shown by more positive δD_{Precip} during 0.52–0.36 Ma should also favor increased dust emissions, yet lower dust fluxes are observed. The more northerly position of ecosystem ranges in the 0.52–0.36 Ma window necessitates a contraction of the Sahara, and thus a smaller dust

source area, implying that some of the decrease in dust flux between 1.1–1.0 Ma and 0.52–0.36 Ma may have been due to contracted dust source areas. However, dust flux declines a further ∼28% between 0.52–0.36 Ma and 0.24–0 Ma despite more southerly ecosystem ranges and expanding dust source areas. Thus, the availability of fine-grained sediments—not aridity, wind strength, nor dust source area size—appears to have driven this declining dust flux trend over the last 1.1 Ma. New fine-grained sediments are produced by fluvial activity and lake development during wet monsoon intervals (Trauth et al., 2009). When monsoon strength declined between 1.1–1.0 Ma and 0.52–0.36 Ma the new weaker monsoon baseline resulted in less fine-grain sediment production during wet monsoon intervals. Over time, the loss of these fine-grained sediments from deflation outpaced new fine-grained sediment production leading to progressive declines in dust flux. Similar declines in dust flux to the North Pacific Ocean over the Plio-Pleistocene have been attributed to the same mechanism, suggesting that the observed dust flux decline from the Sahara may in fact be part of a larger global pattern (Abell et al., 2023). However, not all marine Plio-Pleistocene dust records agree. For example, records from the central North Atlantic (Naafs et al., 2012) and the Atlantic sector of the Southern Ocean (Martínez-Garcia et al., 2011) both exhibit enhanced dust fluxes during the late-Pleistocene compared to both the Pliocene and early- to mid-Pleistocene. These discrepancies may arise due to the differences in fine grained sediment production between dust source regions dominated by monsoonal climates (e.g., East Asia and North Africa) and those dominated by glacial processes (e.g., Patagonia and North America) (Abell et al., 2023). Future work is thus required to constrain global scale trends in dust fluxes over the Plio-Pleistocene with careful attention paid to both the methods employed for dust flux estimations and the contrasting sedimentary processes controlling fine grained sediment availability among major global dust source regions.

Strong modulation of North African rainfall and dustiness by astronomical variability as well as generally lower rainfall in the Pleistocene compared to the Pliocene are common among all the records discussed here, yet the timing, nature, and spatial variability of the transition from a wet Pliocene North Africa to the dry modern North Africa remains poorly constrained. Future work generating high-resolution records of δD_{Precip} from marine sediments off Northwest Africa and in the Eastern Mediterranean will be critical to determining whether the nature of this transition was abrupt or gradual and spatially homogenous or heterogenous. By focusing on both the western and eastern reaches of the continent, such studies will be able to shed light on potential differences in the drivers of precipitation in western versus eastern North Africa which may be related to changes in atmospheric circulation (e.g., the strength of the TEJ vs. AEJ); Indian versus Atlantic Ocean overturning circulation, SSTs, or SST gradients; or more distal forcings such as Pacific Ocean-driven shifts in the strength of tropical Walker circulation and variable teleconnections.

5.4. Plio-Pleistocene Evolution of Northwest African Vegetation

During the Pliocene, much of the modern-day Saharan latitudes were covered by extensive grassland and savanna ecosystems with tropical forests expanded into what is currently occupied by savannas (Berntell et al., 2021; Cerling et al., 1997; Feakins et al., 2013; Leroy & Dupont, 1994; Novello et al., 2015; Ruddiman et al., 1989; Salzmann et al., 2008; Vallé et al., 2014; Zhang et al., 2019). If hydroclimate alone determines ecosystem distributions, one would expect the ranges of these ecosystems to contract equatorward in turn with reductions in monsoon strength over the Plio-Pleistocene (Figure 5b). This would manifest as a shift toward grassier vegetation, recorded by more positive $\delta^{13}C_{wax}$ values following the monsoon strength decline between 1.0 and 0.52 Ma. However, this is not what is observed. Between 3.0 and 1.1 Ma, $\delta^{13}C_{wax}$ values increased by ∼+1.5‰ indicating a shift toward grassier vegetation predates the monsoon rainfall decline (Figure 6a). Low resolution $\delta^{13}C_{wax}$ data from the Northwest African margin show these more positive $\delta^{13}C_{wax}$ values observed during 1.1–1.0 Ma may have been the culmination of a ca. 2 Myr shift toward grassier vegetation (Figure 6a). As discussed in the previous section, an early stage of increased dust flux in North Africa likely occurred ca. 3.2 Ma, however this was likely due to changes in monsoon rainfall distributions, or changes in winds rather than a mean state decline in the West African monsoon rainfall. The shift toward more grassy vegetation in Northwest Africa between 3 and 1.1 Ma in the absence of a coincidently large decline in monsoon rainfall suggests other drivers must be more important. Moreover, across the three Pleistocene time slices, the shifting sensitivities between rainfall and CO_2 on $\delta^{13}C_{wax}$ indicate ecosystem ranges shifted independent of changes in monsoon rainfall, with the rainiest interval (1.1–1.0 Ma) exhibiting the southern-most, not northern-most, ecosystem positions (Figure 3). While it is possible that falling atmospheric CO_2 levels between the Pliocene and mid-Pleistocene resulted in decreased woody cover in North African landscapes (Bond & Midgley, 2000; Bragg et al., 2013; Ehleringer et al., 1997; O'Mara et al., 2022;

Stevens et al., 2016; Yamamoto et al., 2022), the migrations of ecosystems between the two late-Pleistocene time slices without a change in mean rainfall or mean atmospheric CO_2 conflict with this mechanism. Reconstructions of the desert/savanna and savanna/forest boundary spanning the last 0.7 Ma determined using a transect of pollen records along the Northwest African margin show a clear southward shift ca. 0.25 Ma (Figure 6c).

Changes in core sedimentology and pollen fluxes are consistent with broadly southward shifts in ecosystem ranges since the Pliocene. Shifts toward higher ln(Fe/K) values in ODP site 659 sediments have been interpreted to represent a southerly shift in dust source regions across three time slices spanning the Pliocene to late-Pleistocene (5.0–4.6, 3.6–2.5, 0.14–0 Ma) (Vallé et al., 2014) (Figure 6d). Potassium is leached from soils by chemical weathering resulting in progressively higher Fe/K ratios in soils that receive high rainfall (Govin et al., 2012). Accordingly, Saharan soils have low Fe/K ratios, savanna soils have high Fe/K ratios, and Sahelian grassland soils have intermediate Fe/K ratios (Mulitza et al., 2008). This Plio-Pleistocene increase in ln(Fe/K) in ODP 659 sediments was reportedly caused by southward shifts in ecosystem ranges toward more weathered soils that are depleted in potassium. As vegetation retreated southward more soils with higher Fe/K ratios were exposed, deflated, and transported to ODP site 659 as dust. Recently published data from the same core filled in previous gaps in the ln(Fe/K) record showing this retreat was gradual over the duration of the Plio-Pleistocene (Crocker et al., 2022) (Figure 6d). Moreover, the total fluxes of pollen from savanna, forest, and woodland taxa to ODP site 659 have generally declined since the Pliocene, rebounding briefly in the mid-Pleistocene contemporaneous with more northerly ecosystem positions inferred from the relationships between $\delta^{13}C_{wax}$ and $CO_2/\delta D_{Precip}$ (Figure 6c).

We suggest two possible explanations for the disconnect between the latitude of vegetation zones and monsoon rainfall. First, δD_{Precip} records changes in monsoon rainfall amount not necessarily the spatial or seasonal distribution of monsoon rainfall. It is possible that despite the similar δD_{Precip} values between the Pliocene intervals (5.0–4.6 Ma and 3.6–3.0 Ma) and our new MPT interval (1.1–1.0 Ma), monsoon rainfall may have penetrated deeper into the North African interior or fallen over longer wet seasons during the Pliocene (De Boer et al., 2021; Heslop et al., 2023). Increased ventilation by subtropical airmasses as Northern Hemisphere ice sheets developed may have served as an increasingly strong barrier to the penetration of monsoon moisture along its northern edge, as suggested by some climate model simulations (Chou & Neelin, 2003). However, this mechanism cannot explain the dominant precession and obliquity pacing of Northwest African hydroclimate observed in the late-Pleistocene. Thus, is it difficult to reconcile how this ventilation mechanism would apply on million-year timescales, but not glacial-interglacial timescales. Second, changes in ecosystem disturbance by herbivory or fire could have acted to hasten woody cover retreat (Archibald & Hempson, 2016; Bond et al., 2005; Sankaran et al., 2005). While the relationships between wildfires and herbivory on ecosystem compositions are a focus of modern ecological studies (Lehmann et al., 2014; Sankaran et al., 2005; Staver et al., 2011) how these processes may have influenced shifting ecosystem distributions on paleo-timescales has received much less attention (Karp et al., 2021). Long and continuous records of fire and herbivory in North African ecosystems are needed to resolve this conundrum.

5.5. Opal Fluxes Implicate Fe Fertilization Control on Marine Productivity

Dust and opal fluxes exhibit a consistent trend over three mid- to late-Pleistocene time slices, which points to an important role of marine productivity fertilization by dust off the Northwest African margin (Figure 7). In the modern Canary Current upwelling system, nutrients are delivered to the surface ocean from (a) upwelling of remineralized subsurface waters and (b) dust deposition from Saharan dust outbreak events (Fischer, Karakas, et al., 2009; Fischer, Reuter, et al., 2009; Fischer et al., 2016, 2019; Ohde & Siegel, 2010). On millennial to astronomical timescales, the relative importance of upwelling versus dust delivery on surface ocean nutrient supplies are difficult to disentangle as both co-vary with, and are likely mutually determined by, changes in the strength of the trade winds which wax/wane during dry/wet monsoon states.

Our windowed analysis of the last 1.1 Ma shows that over this interval, opal fluxes progressively decline in step with dust fluxes (Figure 7) under the backdrop of increases in global wind speeds. In North Africa, trade winds intensified beginning ca. 2.7 Ma, increasing in strength over the last 2.5 Ma (Vallé et al., 2014). Increased trade wind strength should result in enhanced coastal upwelling along the Northwest African margin, which could act to increase primary productivity. However, opal fluxes declined over this time. Thus, the simultaneous decline in opal and dust flux suggests that declining nutrient loads from dust outweighed any increased nutrient loading from

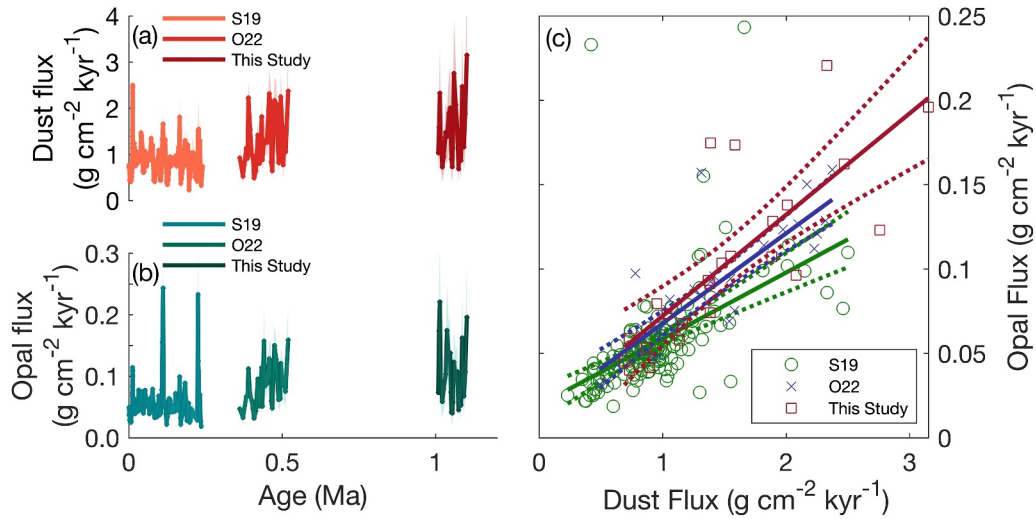

Figure 7. Pleistocene records of dust and opal flux. (a) Northwest African margin (MD03-2705) CFP-normalized dust fluxes from Skonieczny et al. (2019) ($^{230}Th_{XS}$), (O'Mara et al., 2022) ($^{3}He_{ET}$), and this study ($^{3}He_{ET}$), 1σ uncertainty shown in shading. (b) as in (a) but for opal flux. (c) cross-plots and linear regressions of dust versus opal flux for each time slice in (a)/(b).

enhanced wind-driven upwelling. Declining dust deposition of key nutrients including Fe, Si, and P was therefore the dominant control on surface ocean primary productivity in the Canary Current upwelling system on 10^5–10^6-year timescales.

6. Conclusions

We present new reconstructions of monsoon rainfall intensity (from δD_{Precip}), vegetation composition (from landscape C_3/C_4 balance, inferred from $\delta^{13}C_{wax}$), and changes in terrestrial dust emissions and marine productivity (from $^{3}He_{ET}$-normalized dust and opal fluxes) in Northwest Africa during the Mid-Pleistocene Transition (1.1–1.0 Ma). Putting these new records in context with previously published literature, we find that the tempo and amplitude of Northwest African monsoon variability over the last 5 Ma has been consistently governed by changes in precession and obliquity. However, long-term changes in monsoon intensity are not caused by astronomical forcing. Northwest African monsoon intensity was high during the Pliocene until the mid-Pleistocene when rainfall intensity declined sometime between 1.0 and 0.52 Ma. The cause of this shift toward more arid conditions in Northwest Africa remains uncertain. The most likely explanation is the increase in the North Atlantic meridional SST gradient associated with Mid-Pleistocene Transition cooling of the North Atlantic or a decline in AMOC strength since the Pliocene.

Our results demonstrate that grassland, savanna, and forest ecosystems reached farther northward into the Sahara during the warmer, wetter, and higher CO_2 Pliocene. However, long-term ecosystem distributions do not appear to be controlled primarily by changes in monsoon intensity, temperature, or CO_2. Changes in the northward penetration of the monsoon system into the North African continental interior or changes in the degree of ecosystem disturbances by herbivory or fire may thus play a previously underappreciated role in setting the distribution of Northwest African biomes on hundreds of thousands to million-year timescales.

Finally, constant flux normalized sediment accumulation records exhibit a decreasing trend over the last 1.1 Ma suggesting that decreased fine-grained sediment production by a weaker monsoon following the MPT led to progressive declines in dust availability. The tight coupling between dust and opal flux within and across these Pleistocene time slices show that nutrient delivery to the surface ocean via dust deposition has been an important driver of marine productivity both on astronomical and million-year timescales.

Data Availability Statement

All data generated in this study can be found in the supporting data files and archived on figshare.com (https://doi.org/10.6084/m9.figshare.26004421) O'Mara 2024.

Acknowledgments
IMAGES core MD03-2705 was recovered by the R/V Marion Dufresne (Institut Paul Emile Victor) in 2003. These authors would like to acknowledge the National Science Foundation (award #1502925) for funding and Nicole deRoberts, Helen Habicht, Linda Baker, Martin Stute, Stephen Cox, Jenny Middleton, Sidney Hemming for laboratory assistance, David Naafs, Udara Amarathunga, and an anonymous referee for constructive comments which greatly improved the manuscript. C.S. was partly supported by the French national program LEFE/INSU. G.W. acknowledges support from the Vetlesen Foundation.

References

Abell, J. T., Winckler, G., Anderson, R. F., & Herbert, T. D. (2021). Poleward and weakened westerlies during Pliocene warmth. *Nature*, *589*(7840), 70–75. https://doi.org/10.1038/s41586-020-03062-1

Abell, J. T., Winckler, G., Pullen, A., Kinsley, C. W., Kapp, P. A., Middleton, J. L., et al. (2023). Evaluating the drivers of quaternary dust fluxes to the western North Pacific: East Asian dustiness and northern hemisphere gustiness. *Paleoceanography and Paleoclimatology*, *38*(9). https://doi.org/10.1029/2022PA004571

Almogi-Labin, A. (2011). The paleoclimate of the Eastern Mediterranean during the transition from early to mid Pleistocene (900 to 700ka) based on marine and non-marine records: An integrated overview. *Journal of Human Evolution*, *60*(4), 428–436. https://doi.org/10.1016/j.jhevol.2010.03.007

Archibald, S., & Hempson, G. P. (2016). Competing consumers: Contrasting the patterns and impacts of fire and mammalian herbivory in Africa. *Philosophical Transactions of the Royal Society B: Biological Sciences*, *371*(1703), 20150309. https://doi.org/10.1098/rstb.2015.0309

Baas, M., Pancost, R., Van Geel, B., & Sinninghe Damsté, J. S. (2000). A comparative study of lipids in Sphagnum species. *Organic Geochemistry*, *31*(6), 535–541. https://doi.org/10.1016/S0146-6380(00)00037-1

Badewien, T., Vogts, A., & Rullkötter, J. (2015). n-Alkane distribution and carbon stable isotope composition in leaf waxes of C_3 and C_4 plants from Angola. *Organic Geochemistry*, *89–90*, 71–79. https://doi.org/10.1016/j.orggeochem.2015.09.002

Berger, A. L. (1978). Long-term variations of daily insolation and Quaternary climatic changes. *Journal of the Atmospheric Sciences*, *35*(12), 2361–2367. https://doi.org/10.1175/1520-0469(1978)035<2362:ltvodi>2.0.co;2

Berger, A. L., & Loutre, M. F. (1991). Insolation values for the climate of the last 10 million years. *Quaternary Science Reviews*, *10*(4), 297–317. https://doi.org/10.1016/0277-3791(91)90033-Q

Berntell, E., Zhang, Q., Li, Q., Haywood, A. M., Tindall, J. C., Hunter, S. J., et al. (2021). Mid-Pliocene West African monsoon rainfall as simulated in the PlioMIP2 ensemble. *Climate of the Past*, *17*(4), 1777–1794. https://doi.org/10.5194/cp-17-1777-2021

Bezabih, M., Pellikaan, W. F., Tolera, A., & Hendriks, W. H. (2011). Evaluation of n-alkanes and their carbon isotope enrichments ($\delta^{13}C$) as diet composition markers. *Animal, The International Journal of Animal Biosciences*, *5*(1), 57–66. https://doi.org/10.1017/S1751731110001515

Biasutti, M. (2019). Rainfall trends in the African Sahel: Characteristics, processes, and causes. *WIREs Climate Change*, *10*(4), e591. https://doi.org/10.1002/wcc.591

Bond, W. J., & Midgley, G. F. (2000). A proposed CO_2-controlled mechanism of woody plant invasion in grasslands and savannas. *Global Change Biology*, *6*(8), 865–869. https://doi.org/10.1046/j.1365-2486.2000.00365.x

Bond, W. J., Woodward, F. I., & Midgley, G. F. (2005). The global distribution of ecosystems in a world without fire. *New Phytologist*, *165*(2), 525–538. https://doi.org/10.1111/j.1469-8137.2004.01252.x

Bosmans, J. H. C., Drijfhout, S. S., Tuenter, E., Hilgen, F. J., & Lourens, L. J. (2015). Response of the North African summer monsoon to precession and obliquity forcings in the EC-Earth GCM. *Climate Dynamics*, *44*(1–2), 279–297. https://doi.org/10.1007/s00382-014-2260-z

Bosmans, J. H. C., Hilgen, F. J., Tuenter, E., & Lourens, L. J. (2015). Obliquity forcing of low-latitude climate. *Climate of the Past*, *11*(10), 1335–1346. https://doi.org/10.5194/cp-11-1335-2015

Bradtmiller, L. I., McGee, D., Awalt, M., Evers, J., Yerxa, H., Kinsley, C. W., & DeMenocal, P. B. (2016). Changes in biological productivity along the northwest African margin over the past 20,000 years. *Paleoceanography*, *31*(1), 185–202. https://doi.org/10.1002/2015PA002862

Bragg, F. J., Prentice, I. C., Harrison, S. P., Eglinton, G., Foster, P. N., Rommerskirchen, F., & Rullkötter, J. (2013). Stable isotope and modelling evidence for CO_2 as a driver of glacial-interglacial vegetation shifts in southern Africa. *Biogeosciences*, *10*(3), 2001–2010. https://doi.org/10.5194/bg-10-2001-2013

Bridges, J. D., Tarduno, J. A., Cottrell, R. D., & Herbert, T. D. (2023). Rapid strengthening of westerlies accompanied intensification of Northern Hemisphere glaciation. *Nature Communications*, *14*(1), 3905. https://doi.org/10.1038/s41467-023-39557-4

Brierley, C. M., & Fedorov, A. V. (2010). Relative importance of meridional and zonal sea surface temperature gradients for the onset of the ice ages and Pliocene-Pleistocene climate evolution. *Paleoceanography*, *25*(2), 1–16. https://doi.org/10.1029/2009PA001809

Burls, N. J., & Fedorov, A. V. (2017). Wetter subtropics in a warmer world: Contrasting past and future hydrological cycles. *Proceedings of the National Academy of Sciences of the United States of America*, *114*(49), 12888–12893. https://doi.org/10.1073/pnas.1703421114

Bush, R. T., & McInerney, F. A. (2013). Leaf wax *n*-alkane distributions in and across modern plants: Implications for paleoecology and chemotaxonomy. *Geochimica et Cosmochimica Acta*, *117*, 161–179. https://doi.org/10.1016/j.gca.2013.04.016

Bush, R. T., & McInerney, F. A. (2015). Influence of temperature and C_4 abundance on *n*-alkane chain length distributions across the central USA. *Organic Geochemistry*, *79*, 65–73. https://doi.org/10.1016/j.orggeochem.2014.12.003

Castañeda, I. S., Mulitza, S., Schefuß, E., Dos Santos, R. A. L., Damsté, J. S. S., & Schouten, S. (2009). Wet phases in the Sahara/Sahel region and human migration patterns in North Africa. *Proceedings of the National Academy of Sciences of the United States of America*, *106*(48), 20159–20163. https://doi.org/10.1073/pnas.0905771106

Cenozoic CO2 Proxy Integration Project (CenCO2PIP) Consortium, Hönisch, B., Hönisch, B., Royer, D. L., Breecker, D. O., Polissar, P. J., et al. (2023). Toward a Cenozoic history of atmospheric CO_2. *Science*, *382*(6675), eadi5177. https://doi.org/10.1126/science.adi5177

Cerling, T. E., & Harris, J. M. (1999). Carbon isotope fractionation between diet and bioapatite in ungulate mammals and implications for ecological and paleoecological studies. *Oecologia*, *120*(3), 347–363. https://doi.org/10.1007/s004420050868

Cerling, T. E., Harris, J. M., MacFadden, B. J., Leakey, M. G., Quade, J., Eisenmann, V., & Ehleringer, J. R. (1997). Global vegetation change through the Miocene/Pliocene boundary. *Nature*, *389*(6647), 153–158. https://doi.org/10.1038/38229

Chandan, D., & Peltier, W. R. (2020). African humid period precipitation sustained by robust vegetation, soil, and lake feedbacks. *Geophysical Research Letters*, *47*(21). https://doi.org/10.1029/2020GL088728

Chou, C., & Neelin, J. D. (2003). Mechanisms limiting the northward extent of the northern summer monsoons over North America, Asia, and Africa. *Journal of Climate*, *16*(3), 406–425. https://doi.org/10.1175/1520-0442(2003)016<0406:MLTNEO>2.0.CO;2

Claussen, M., Dallmeyer, A., & Bader, J. (2017). In *Theory and modeling of the African humid period and the Green Sahara* (Vol. 1). Oxford University Press. https://doi.org/10.1093/acrefore/9780190228620.013.532

Costa, K. M., Hayes, C. T., Anderson, R. F., Pavia, F. J., Bausch, A., Deng, F., et al. (2020). 230Th normalization: New insights on an essential tool for quantifying sedimentary fluxes in the modern and quaternary ocean. *Paleoceanography and Paleoclimatology*, *35*(2), 1–36. https://doi.org/10.1029/2019PA003820

Crocker, A. J., Naafs, B. D. A., Westerhold, T., James, R. H., Cooper, M. J., Röhl, U., et al. (2022). Astronomically controlled aridity in the Sahara since at least 11 million years ago. *Nature Geoscience*, *15*(8), 671–676. https://doi.org/10.1038/s41561-022-00990-7

Dallmeyer, A., Claussen, M., Lorenz, S. J., & Shanahan, T. (2020). The end of the African humid period as seen by a transient comprehensive Earth system model simulation of the last 8000 years. *Climate of the Past*, *16*(1), 117–140. https://doi.org/10.5194/cp-16-117-2020

Dansgaard, W. (1964). Stable isotopes in precipitation. *Tellus*, *16*(4), 436–468. https://doi.org/10.1111/j.2153-3490.1964.tb00181.x

De Boer, B., Peters, M., & Lourens, L. J. (2021). The transient impact of the African monsoon on Plio-Pleistocene Mediterranean sediments. *Climate of the Past*, *17*(1), 331–344. https://doi.org/10.5194/cp-17-331-2021

De La Vega, E., Chalk, T. B., Wilson, P. A., Bysani, R. P., & Foster, G. L. (2020). Atmospheric CO_2 during the mid-Piacenzian Warm Period and the M2 glaciation. *Scientific Reports*, *10*(1), 11002. https://doi.org/10.1038/s41598-020-67154-8

de Menocal, P. B. (1995). Plio-Pleistocene african climate. *Science*, *270*(5233), 53–59. https://doi.org/10.1126/science.270.5233.53

de Menocal, P. B. (2004). African climate change and faunal evolution during the Pliocene-Pleistocene. *Earth and Planetary Science Letters*, *220*(1–2), 3–24. https://doi.org/10.1016/S0012-821X(04)00003-2

Dowsett, H., Robinson, M., Haywood, A. M., Salzmann, U., Hill, D., Sohl, L. E., et al. (2010). The PRISM3D paleoenvironmental reconstruction. *Stratigraphy*, *7*(2–3), 123–139. https://doi.org/10.29041/strat.07.2.03

Dupont, L. M. (1993). Vegetation zones in NW Africa during the brunhes chron reconstructed from marine palynological data. *Quaternary Science Reviews*, *12*(3), 189–202. https://doi.org/10.1016/0277-3791(93)90053-O

Dupont, L. M., Donner, B., Schneider, R., & Wefer, G. (2001). Mid-Pleistocene environmental change in tropical Africa began as early as 1.05 Ma. *Geology*, *29*(3), 195–198. https://doi.org/10.1130/0091-7613(2001)029<0195:MPECIT>2.0.CO;2

Duque-Villegas, M., Claussen, M., Brovkin, V., & Kleinen, T. (2022). Effects of orbital forcing, greenhouse gases and ice sheets on Saharan greening in past and future multi-millennia. *Climate of the Past*, *18*(8), 1897–1914. https://doi.org/10.5194/cp-18-1897-2022

Dyez, K. A., Hönisch, B., & Schmidt, G. A. (2018). Early Pleistocene obliquity-scale pCO_2 variability at ∼1.5 million years ago. *Paleoceanography and Paleoclimatology*, *33*(11), 1270–1291. https://doi.org/10.1029/2018PA003349

Ebisuzaki, W. (1997). A method to estimate the statistical significance of a correlation when the data are serially correlated. *Journal of Climate*, *10*(9), 2147–2153. https://doi.org/10.1175/1520-0442(1997)010<2147:AMTETS>2.0.CO;2

Eglinton, G., & Hamilton, R. J. (1967). Leaf epicuticular waxes: The waxy outer surfaces of most plants display a wide diversity of fine structure and chemical constituents. *Science*, *156*(3780), 1322–1335. https://doi.org/10.1126/science.156.3780.1322

Ehleringer, J. R., Cerling, T. E., & Helliker, B. R. (1997). C4 photosynthesis, atmospheric CO2, and climate. *Oecologia*, *112*(3), 285–299. https://doi.org/10.3760/cma.j.issn.0254-6450.2011.05.005

Eisenman, I., & Huybers, P. J. (2006). daily_insolation.

Farley, K. A. (2001). Extraterrestrial helium in seafloor sediments: Identification, characteristics, and accretion rate over geologic time. In *Accretion of extraterrestrial matter throughout Earth's history* (pp. 179–204). Springer US. https://doi.org/10.1007/978-1-4419-8694-8_11

Feakins, S. J., Levin, N. E., Liddy, H. M., Sieracki, A., Eglinton, T. I., & Bonnefille, R. (2013). Northeast African vegetation change over 12 m.y. *Geology*, *41*(3), 295–298. https://doi.org/10.1130/G33845.1

Fedorov, A. V., Brierley, C. M., Lawrence, K. T., Liu, Z., Dekens, P. S., & Ravelo, A. C. (2013). Patterns and mechanisms of early Pliocene warmth. *Nature*, *496*(7443), 43–49. https://doi.org/10.1038/nature12003

Ficken, K. J., Li, B., Swain, D., & Eglinton, G. (2000). An *n*-alkane proxy for the sedimentary input of submerged/floating freshwater aquatic macrophytes. *Organic Geochemistry*, *31*(7–8), 745–749. https://doi.org/10.1016/s0146-6380(00)00081-4

Fischer, G., Karakas, G., Blaas, M., Ratmeyer, V., Nowald, N., Schlitzer, R., et al. (2009). Mineral ballast and particle settling rates in the coastal upwelling system off NW Africa and the South Atlantic. *International Journal of Earth Sciences*, *98*(2), 281–298. https://doi.org/10.1007/s00531-007-0234-7

Fischer, G., Reuter, C., Karakas, G., Nowald, N., & Wefer, G. (2009). Offshore advection of particles within the Cape Blanc filament, Mauritania: Results from observational and modelling studies. *Progress in Oceanography*, *83*(1–4), 322–330. https://doi.org/10.1016/j.pocean.2009.07.023

Fischer, G., Romero, O., Merkel, U., Donner, B., Iversen, M., Nowald, N., et al. (2016). Deep ocean mass fluxes in the coastal upwelling off Mauritania from 1988 to 2012: Variability on seasonal to decadal timescales. *Biogeosciences*, *13*(10), 3071–3090. https://doi.org/10.5194/bg-13-3071-2016

Fischer, G., Romero, O., Toby, E., Iversen, M., Donner, B., Mollenhauer, G., et al. (2019). Changes in the dust-influenced biological carbon pump in the canary current system: Implications from a coastal and an offshore sediment trap record off Cape Blanc, Mauritania. *Global Biogeochemical Cycles*, *33*(8), 1100–1128. https://doi.org/10.1029/2019GB006194

Garcin, Y., Schefuß, E., Schwab, V. F., Garreta, V., Gleixner, G., Vincens, A., et al. (2014). Reconstructing C_3 and C_4 vegetation cover using n-alkane carbon isotope ratios in recent lake sediments from Cameroon, Western Central Africa. *Geochimica et Cosmochimica Acta*, *142*, 482–500. https://doi.org/10.1016/J.GCA.2014.07.004

Ginoux, P., Prospero, J. M., Gill, T. E., Hsu, N. C., & Zhao, M. (2012). Global-scale attribution of anthropogenic and natural dust sources and their emission rates based on MODIS Deep Blue aerosol products. *Reviews of Geophysics*, *50*(3), 1–36. https://doi.org/10.1029/2012RG000388

Govin, A., Holzwarth, U., Heslop, D., Ford Keeling, L., Zabel, M., Mulitza, S., et al. (2012). Distribution of major elements in Atlantic surface sediments (36°N–49°S): Imprint of terrigenous input and continental weathering. *Geochemistry, Geophysics, Geosystems*, *13*(1), 1–23. https://doi.org/10.1029/2011GC003785

Grant, K. M., Amarathunga, U., Amies, J. D., Hu, P., Qian, Y., Penny, T., et al. (2022). Organic carbon burial in Mediterranean sapropels intensified during Green Sahara Periods since 3.2 Myr ago. *Communications Earth & Environment*, *3*(1), 11. https://doi.org/10.1038/s43247-021-00339-9

Grist, J. P., & Nicholson, S. E. (2001). A study of the dynamic factors influencing the rainfall variability in the West African Sahel. *Journal of Climate*, *14*(7), 1337–1359. https://doi.org/10.1175/1520-0442(2001)014<1337:ASOTDF>2.0.CO;2

Grodsky, S. A., Carton, J. A., & Nigam, S. (2003). Near surface westerly wind jet in the Atlantic ITCZ. *Geophysical Research Letters*, *30*(19), 2003GL017867. https://doi.org/10.1029/2003GL017867

Haywood, A. M., Dowsett, H. J., Otto-Bliesner, B., Chandler, M. A., Dolan, A. M., Hill, D. J., et al. (2010). Pliocene model intercomparison project (PlioMIP): Experimental design and boundary conditions (Experiment 1). *Geoscientific Model Development*, *3*(1), 227–242. https://doi.org/10.5194/gmd-3-227-2010

Haywood, A. M., Hill, D. J., Dolan, A. M., Otto-Bliesner, B. L., Bragg, F., Chan, W.-L., et al. (2013). Large-scale features of Pliocene climate: Results from the pliocene model intercomparison project. *Climate of the Past*, *9*(1), 191–209. https://doi.org/10.5194/cp-9-191-2013

Haywood, A. M., Tindall, J. C., Dowsett, H. J., Dolan, A. M., Foley, K. M., Hunter, S. J., et al. (2020). The pliocene model Intercomparison project phase 2: Large-scale climate features and climate sensitivity. *Climate of the Past*, *16*(6), 2095–2123. https://doi.org/10.5194/cp-16-2095-2020

Hély, C., Lézine, A. M., Ballouche, A., Cour, P., Duzer, D., Guinet, P., et al. (2014). Holocene changes in African vegetation: Tradeoff between climate and water availability. *Climate of the Past*, *10*(2), 681–686. https://doi.org/10.5194/cp-10-681-2014

Hennekam, R., Grant, K. M., Rohling, E. J., Tjallingii, R., Heslop, D., Roberts, A. P., et al. (2022). Accurately calibrated X-ray fluorescence core scanning (XRF-CS) record of Ti/Al reveals Early Pleistocene aridity and humidity variability over North Africa and its close relationship to low-latitude insolation. *Climate of the Past*, *18*(11), 2509–2521. https://doi.org/10.5194/cp-18-2509-2022

Herbert, T. D., Peterson, L. C., Lawrence, K. T., & Liu, Z. (2010). Tropical ocean temperatures over the past 3.5 million years. *Science*, *328*(5985), 1530–1534. https://doi.org/10.1126/science.1185435

Heslop, D., Amarathunga, U., & Rohling, E. J. (2023). Estimating Plio-Pleistocene North African monsoon runoff into the Mediterranean Sea and temperature impacts. *Paleoceanography and Paleoclimatology*, *38*(11), e2023PA004677. https://doi.org/10.1029/2023PA004677

Higgins, J. A., Kurbatov, A. V., Spaulding, N. E., Brook, E., Introne, D. S., Chimiak, L. M., et al. (2015). Atmospheric composition 1 million years ago from blue ice in the Allan Hills, Antarctica. *Proceedings of the National Academy of Sciences of the United States of America*, *112*(22), 6887–6891. https://doi.org/10.1073/pnas.1420232112

Hooghiemstra, H., Lézine, A. M., Leroy, S. A. G., Dupont, L., & Marret, F. (2006). Late Quaternary palynology in marine sediments: A synthesis of the understanding of pollen distribution patterns in the NW African setting. *Quaternary International*, *148*(1), 29–44. https://doi.org/10.1016/j.quaint.2005.11.005

Huang, Y., Dupont, L., Sarnthein, M., Hayes, J. M., & Eglinton, G. (2000). Mapping of C4 plant input from north West Africa into north East Atlantic sediments. *Geochimica et Cosmochimica Acta*, *64*(20), 3505–3513. https://doi.org/10.1016/s0016-7037(00)00445-2

Jolly, D., Prentice, I. C., Bonnefille, R., Ballouche, A., Bengo, M., Brenac, P., et al. (1998). Biome reconstruction from pollen and plant macrofossil data for Africa and the Arabian peninsula at 0 and 6000 years. *Journal of Biogeography*, *25*(6), 1007–1027. https://doi.org/10.1046/j.1365-2699.1998.00238.x

Jullien, E., Grousset, F., Malaizé, B., Duprat, J., Sanchez-Goni, M. F., Eynaud, F., et al. (2007). Low-latitude "dusty events" vs. high-latitude "icy Heinrich events". *Quaternary Research*, *68*(3), 379–386. https://doi.org/10.1016/J.YQRES.2007.07.007

Karp, A. T., Faith, T. J., Marlon, J. R., & Staver, C. A. (2021). Global response of fire activity to late Quaternary grazer extinctions. *Science*, *374*(6571), 1145–1148. https://doi.org/10.1126/science.abj1580

Kim, J., Goldstein, S. L., Pena, L. D., Jaume-Seguí, M., Knudson, K. P., Yehudai, M., & Bolge, L. (2021). North Atlantic deep water during Pleistocene interglacials and glacials. *Quaternary Science Reviews*, *269*, 107146. https://doi.org/10.1016/j.quascirev.2021.107146

Kristen, I., Wilkes, H., Vieth, A., Zink, K.-G., Plessen, B., Thorpe, J., et al. (2010). Biomarker and stable carbon isotope analyses of sedimentary organic matter from Lake Tswaing: Evidence for deglacial wetness and early Holocene drought from South Africa. *Journal of Paleolimnology*, *44*(1), 143–160. https://doi.org/10.1007/s10933-009-9393-9

Kuechler, R. R., Dupont, L. M., & Schefuß, E. (2018). Hybrid insolation forcing of Pliocene monsoon dynamics in West Africa. *Climate of the Past*, *14*(1), 73–84. https://doi.org/10.5194/cp-14-73-2018

Kuechler, R. R., Schefuß, E., Beckmann, B., Dupont, L., & Wefer, G. (2013). NW African hydrology and vegetation during the Last Glacial cycle reflected in plant-wax-specific hydrogen and carbon isotopes. *Quaternary Science Reviews*, *82*, 56–67. https://doi.org/10.1016/J.QUASCIREV.2013.10.013

Kutzbach, J. E. (1981). Monsoon climate of the early Holocene: Climate experiment with the earth's orbital parameters for 9000 years ago. *Science*, *214*(4516), 59–61. https://doi.org/10.1126/science.214.4516.59

Kutzbach, J. E., Bonan, G., Foley, J., & Harrison, S. P. (1996). Vegetation and soil feedbacks on the response of the African monsoon to orbital forcing in the early to middle Holocene. *Nature*, *384*(6610), 623–626. https://doi.org/10.1038/384623a0

Larrasoaña, J. C. (2021). A review of West African monsoon penetration during Green Sahara periods; implications for human evolution and dispersals over the last three million years. *Oxford Open Climate Change*, *1*(1), 1–19. https://doi.org/10.1093/oxfclm/kgab011

Larrasoaña, J. C., Roberts, A. P., Rohling, E. J., Winklhofer, M., & Wehausen, R. (2003). Three million years of monsoon variability over the northern Sahara. *Climate Dynamics*, *21*(7–8), 689–698. https://doi.org/10.1007/s00382-003-0355-z

Lavaysse, C., Flamant, C., & Janicot, S. (2010). Regional-scale convection patterns during strong and weak phases of the Saharan heat low. *Atmospheric Science Letters*, *11*(4), 255–264. https://doi.org/10.1002/asl.284

Lawrence, K. T., Sosdian, S., White, H. E., & Rosenthal, Y. (2010). North Atlantic climate evolution through the Plio-Pleistocene climate transitions. *Earth and Planetary Science Letters*, *300*(3–4), 329–342. https://doi.org/10.1016/j.epsl.2010.10.013

Lebel, T., & Ali, A. (2009). Recent trends in the Central and Western Sahel rainfall regime (1990–2007). *Journal of Hydrology*, *375*(1–2), 52–64. https://doi.org/10.1016/j.jhydrol.2008.11.030

Lehmann, C. E. R., Anderson, T. M., Sankaran, M., Higgins, S. I., Archibald, S., Hoffmann, W. A., et al. (2014). Savanna vegetation-fire-climate relationships differ among continents. *Science*, *343*(6170), 548–552. https://doi.org/10.1126/science.1247355

Le Quilleuc, M., Bory, A. J., Philippe, S., Derimian, Y., Skonieczny, C., Petit, J., et al. (2021). Major element signatures of silicate dust deposited on the West African margin: Links with transport patterns and provenance regions. *Journal of Geophysical Research: Atmospheres*, *126*(20), e2021JD035030. https://doi.org/10.1029/2021JD035030

Leroy, S., & Dupont, L. (1994). Development of vegetation and continental aridity in northwestern Africa during the Late Pliocene: The pollen record of ODP site 658. *Palaeogeography, Palaeoclimatology, Palaeoecology*, *109*(2–4), 295–316. https://doi.org/10.1016/0031-0182(94)90181-3

Li, X., Jiang, D., Zhang, Z., Zhang, R., Tian, Z., & Yan, Q. (2015). Mid-Pliocene westerlies from PlioMIP simulations. *Advances in Atmospheric Sciences*, *32*(7), 909–923. https://doi.org/10.1007/s00376-014-4171-7

Lisiecki, L. E., & Raymo, M. E. (2005). A Pliocene-Pleistocene stack of 57 globally distributed benthic $\delta^{18}O$ records. *Paleoceanography*, *20*(1), 1–17. https://doi.org/10.1029/2004PA001071

Lloyd, J., Bird, M. I., Vellen, L., Miranda, A. C., Veenendaal, E. M., Djagbletey, G., et al. (2008). Contributions of woody and herbaceous vegetation to tropical savanna ecosystem productivity: A quasi-global estimate. *Tree Physiology*, *28*(3), 451–468. https://doi.org/10.1093/treephys/28.3.451

Lupien, R., Uno, K., Rose, C., de Roberts, N., Hazan, C., De Menocal, P., & Polissar, P. (2023). Low-frequency orbital variations controlled climatic and environmental cycles, amplitudes, and trends in northeast Africa during the Plio-Pleistocene. *Communications Earth & Environment*, *4*(1), 360. https://doi.org/10.1038/s43247-023-01034-7

Lüthi, D., Le Floch, M., Bereiter, B., Blunier, T., Barnola, J.-M. M., Siegenthaler, U., et al. (2008). High-resolution carbon dioxide concentration record 650,000–800,000 years before present. *Nature*, *453*(7193), 379–382. https://doi.org/10.1038/nature06949

Magill, C. R., Ashley, G. M., & Freeman, K. H. (2013). Water, plants, and early human habitats in eastern Africa. *Proceedings of the National Academy of Sciences of the United States of America*, *110*(4), 1175–1180. https://doi.org/10.1073/pnas.1209405109

Malaizé, B., Jullien, E., Tisserand, A., Skonieczny, C., Grousset, E. F., Eynaud, F., et al. (2012). The impact of African aridity on the isotopic signature of Atlantic deep waters across the Middle Pleistocene Transition. *Quaternary Research*, *77*(1), 182–191. https://doi.org/10.1016/j.yqres.2011.09.010

Mantsis, D. F., Lintner, B. R., Broccoli, A. J., Erb, M. P., Clement, A. C., & Park, H.-S. (2014). The response of large-scale circulation to obliquity-induced changes in meridional heating gradients. *Journal of Climate*, *27*(14), 5504–5516. https://doi.org/10.1175/JCLI-D-13-00526.1

Marcantonio, F., Anderson, R. F., Stute, M., Kumar, N., Schlosser, P., & Mix, A. (1996). Extraterrestrial ^{3}He as a tracer of marine sediment transport and accumulation. *Nature*, *383*(6602), 705–707. https://doi.org/10.1038/383705a0

Martínez-Botí, M. A., Foster, G. L., Chalk, T. B., Rohling, E. J., Sexton, P. F., Lunt, D. J., et al. (2015). Plio-Pleistocene climate sensitivity evaluated using high-resolution CO_2 records. *Nature*, *518*(7537), 49–54. https://doi.org/10.1038/nature14145

Martínez-Garcia, A., Rosell-Melé, A., Jaccard, S. L., Geibert, W., Sigman, D. M., & Haug, G. H. (2011). Southern Ocean dust–climate coupling over the past four million years. *Nature*, *476*(7360), 312–315. https://doi.org/10.1038/nature10310

McGee, D., Broecker, W. S., & Winckler, G. (2010). Gustiness: The driver of glacial dustiness? *Quaternary Science Reviews*, *29*(17–18), 2340–2350. https://doi.org/10.1016/j.quascirev.2010.06.009

McGee, D., DeMenocal, P. B., Winckler, G., Stuut, J. B. W., Bradtmiller, L. I., de Menocal, P. B., et al. (2013). The magnitude, timing and abruptness of changes in North African dust deposition over the last 20,000 yr. *Earth and Planetary Science Letters*, *371–372*, 163–176. https://doi.org/10.1016/j.epsl.2013.03.054

McGee, D., Moreno-Chamarro, E., Green, B., Marshall, J., Galbraith, E., & Bradtmiller, L. (2018). Hemispherically asymmetric trade wind changes as signatures of past ITCZ shifts. *Quaternary Science Reviews*, *180*, 214–228. https://doi.org/10.1016/j.quascirev.2017.11.020

McGee, D., & Mukhopadhyay, S. (2013). Extraterrestrial he in sediments: From recorder of asteroid collisions to timekeeper of global environmental changes. In *Advances in isotope geochemistry* (pp. 155–176). Springer. https://doi.org/10.1007/978-3-642-28836-4_7

Menviel, L., Govin, A., Avenas, A., Meissner, K. J., Grant, K. M., & Tzedakis, P. C. (2021). Drivers of the evolution and amplitude of African humid periods. *Communications Earth and Environment*, *2*(1), 237. https://doi.org/10.1038/s43247-021-00309-1

Mortlock, R. A., & Froelich, P. N. (1989). A simple method for the rapid determination of biogenic opal in pelagic marine sediments. *Deep-Sea Research, Part A: Oceanographic Research Papers*, *36*(9), 1415–1426. https://doi.org/10.1016/0198-0149(89)90092-7

Mulitza, S., Prange, M., Stuut, J.-B. B., Zabel, M., von Dobeneck, T., Itambi, A. C., et al. (2008). Sahel megadroughts triggered by glacial slowdowns of Atlantic meridional overturning. *Paleoceanography*, *23*(4), 1–11. https://doi.org/10.1029/2008PA001637

Naafs, B. D. A., Hefter, J., Acton, G., Haug, G. H., Martínez-Garcia, A., Pancost, R., & Stein, R. (2012). Strengthening of North American dust sources during the late Pliocene (2.7 Ma). *Earth and Planetary Science Letters*, *317–318*, 8–19. https://doi.org/10.1016/j.epsl.2011.11.026

Naafs, B. D. A., Stein, R., Hefter, J., Khélifi, N., De Schepper, S., & Haug, G. H. (2010). Late Pliocene changes in the North Atlantic Current. *Earth and Planetary Science Letters*, *298*(3–4), 434–442. https://doi.org/10.1016/j.epsl.2010.08.023

Nicholson, S. E. (1980). The nature of rainfall fluctuations in subtropical West Africa. *Monthly Weather Review*, *108*(4), 473–487. https://doi.org/10.1175/1520-0493(1980)108<0473:tnorfi>2.0.co;2

Nicholson, S. E. (2008). The intensity, location and structure of the tropical rainbelt over west Africa as factors in interannual variability. *International Journal of Climatology*, *28*(13), 1775–1785. https://doi.org/10.1002/joc.1507

Nicholson, S. E. (2009). A revised picture of the structure of the "monsoon" and land ITCZ over West Africa. *Climate Dynamics*, *32*(7–8), 1155–1171. https://doi.org/10.1007/s00382-008-0514-3

Nicholson, S. E. (2013). The West African Sahel: A review of recent studies on the rainfall regime and its interannual variability. *ISRN Meteorology*, *2013*, 1–32. https://doi.org/10.1155/2013/453521

Nicholson, S. E. (2018). The ITCZ and the seasonal cycle over equatorial Africa. *Bulletin of the American Meteorological Society*, *99*(2), 337–348. https://doi.org/10.1175/BAMS-D-16-0287.1

Nicholson, S. E., Funk, C., & Fink, A. H. (2018). Rainfall over the African continent from the 19th through the 21st century. *Global and Planetary Change*, *165*, 114–127. https://doi.org/10.1016/j.gloplacha.2017.12.014

Nicholson, S. E., & Palao, I. M. (1993). A re-evaluation of rainfall variability in the Sahel. Part I. Characteristics of rainfall fluctuations. *International Journal of Climatology*, *13*(4), 371–389. https://doi.org/10.1002/joc.3370130403

Niedermeyer, E. M., Forrest, M., Beckmann, B., Sessions, A. L., Mulch, A., & Schefuß, E. (2016). The stable hydrogen isotopic composition of sedimentary plant waxes as quantitative proxy for rainfall in the West African Sahel. *Geochimica et Cosmochimica Acta*, *184*, 55–70. https://doi.org/10.1016/j.gca.2016.03.034

Nier, A. O., & Schlutter, D. J. (1992). Extraction of helium from individual interplanetary dust particles by step-heating. *Meteoritics*, *27*(2), 166–173. https://doi.org/10.1111/j.1945-5100.1992.tb00744.x

Nott, C. J., Xie, S., Avsejs, L. A., Maddy, D., Chambers, F. M., & Evershed, R. P. (2000). n-Alkane distributions in ombrotrophic mires as indicators of vegetation change related to climatic variation. *Organic Geochemistry*, *31*(2–3), 231–235. https://doi.org/10.1016/S0146-6380(99)00153-9

Novello, A., Lebatard, A. E., Moussa, A., Barboni, D., Sylvestre, F., Bourlès, D. L., et al. (2015). Diatom, phytolith, and pollen records from a 10 Be/9 Be dated lacustrine succession in the Chad basin: Insight on the miocene-pliocene paleoenvironmental changes in Central Africa. *Palaeogeography, Palaeoclimatology, Palaeoecology*, *430*, 85–103. https://doi.org/10.1016/j.palaeo.2015.04.013

O'Brien, C. L., Foster, G. L., Martínez-Botí, M. A., Abell, R., Rae, J. W. B., & Pancost, R. D. (2014). High sea surface temperatures in tropical warm pools during the Pliocene. *Nature Geoscience*, *7*(8), 606–611. https://doi.org/10.1038/ngeo2194

Ohde, T., & Siegel, H. (2010). Biological response to coastal upwelling and dust deposition in the area off Northwest Africa. *Continental Shelf Research*, *30*(9), 1108–1119. https://doi.org/10.1016/j.csr.2010.02.016

OMara, N. (2024). Datasets generated for O'Mara et al. (2024), Constraining Plio-Pleistocene shifts in Northwest African hydroclimate, ecosystem distributions, and marine productivity: New paleo-records across the Mid-Pleistocene Transition [Dataset]. *Paleoceanography and Paleoclimatology*. (accepted). figshare. https://doi.org/10.6084/m9.figshare.26004421.v1

O'Mara, N. A., Skonieczny, C., McGee, D., Winckler, G., Bory, A. J.-M., Bradtmiller, L. I., et al. (2022). Pleistocene drivers of Northwest African hydroclimate and vegetation. *Nature Communications*, *13*(1), 3552. https://doi.org/10.1038/s41467-022-31120-x

Orndorff, R. C., Stamm, N. R., Soller, D. R., Edwards, L. E., Herrick, J. A., Ruppert, L. F., et al. (2022). Divisions of geologic time—Major chronostratigraphic and geochronologic units (p. 4). Stratigraphic Notes, 1, 1879–1. https://doi.org/10.3133/pp1879v1

Pagani, M., Liu, Z., Lariviere, J., & Ravelo, A. C. (2010). High Earth-system climate sensitivity determined from Pliocene carbon dioxide concentrations. *Nature Geoscience*, *3*(1), 27–30. https://doi.org/10.1038/ngeo724

Park, J.-Y., Bader, J., & Matei, D. (2015). Northern-hemispheric differential warming is the key to understanding the discrepancies in the projected Sahel rainfall. *Nature Communications*, *6*(1), 5985. https://doi.org/10.1038/ncomms6985

Park, J.-Y., Bader, J., & Matei, D. (2016). Anthropogenic Mediterranean warming essential driver for present and future Sahel rainfall. *Nature Climate Change*, *6*(10), 941–945. https://doi.org/10.1038/nclimate3065

Pausata, F. S. R., Messori, G., & Zhang, Q. (2016). Impacts of dust reduction on the northward expansion of the African monsoon during the Green Sahara period. *Earth and Planetary Science Letters*, *434*, 298–307. https://doi.org/10.1016/j.epsl.2015.11.049

Pena, L. D., & Goldstein, S. L. (2014). Thermohaline circulation crisis and impacts during the mid-Pleistocene transition. *Science*, *345*(6194), 318–322. https://doi.org/10.1126/science.1249770

Pisias, N. G., & Moore, T. C. (1981). The evolution of Pleistocene climate: A time series approach. *Earth and Planetary Science Letters*, *52*(2), 450–458. https://doi.org/10.1016/0012-821x(81)90197-7

Polissar, P. J., & D'Andrea, W. J. (2014). Uncertainty in paleohydrologic reconstructions from molecular δD values. *Geochimica et Cosmochimica Acta*, *129*, 146–156. https://doi.org/10.1016/j.gca.2013.12.021

Polissar, P. J., Rose, C., Uno, K. T., Phelps, S. R., & de Menocal, P. (2019). Synchronous rise of African C_4 ecosystems 10 million years ago in the absence of aridification. *Nature Geoscience*, *12*(8), 657–660. https://doi.org/10.1038/s41561-019-0399-2

Polissar, P. J., Uno, K. T., Phelps, S. R., Karp, A. T., Freeman, K. H., & Pensky, J. L. (2021). Hydrologic changes drove the late miocene expansion of C_4 grasslands on the northern Indian subcontinent. *Paleoceanography and Paleoclimatology*, *36*(4), 1–22. https://doi.org/10.1029/2020PA004108

Prospero, J. M. (1999). Long-term measurements of the transport of African mineral dust to the southeastern United States: Implications for regional air quality. *Journal of Geophysical Research*, *104*(D13), 15917–15927. https://doi.org/10.1029/1999JD900072

Prospero, J. M., & Carlson, T. N. (1972). Vertical and areal distribution of Saharan dust over the western equatorial north Atlantic Ocean. *Journal of Geophysical Research*, *77*(27), 5255–5265. https://doi.org/10.1029/JC077i027p05255

Pu, B., & Cook, K. H. (2010). Dynamics of the West African Westerly Jet. *Journal of Climate*, *23*(23), 6263–6276. https://doi.org/10.1175/2010JCLI3648.1

Rachmayani, R., Prange, M., & Schulz, M. (2016). Intra-interglacial climate variability: Model simulations of marine isotope stages 1, 5, 11, 13, and 15. *Climate of the Past*, *12*(3), 677–695. https://doi.org/10.5194/cp-12-677-2016

Ravelo, A. C., Andreasen, D. H., Lyle, M., Lyle, A. O., & Wara, M. W. (2004). Regional climate shifts caused by gradual global cooling in the Pliocene epoch. *Nature*, *429*(6989), 263–267. https://doi.org/10.1038/nature02567

Raymo, M. E., Hodell, D., & Jansen, E. (1992). Response of deep ocean circulation to initiation of northern hemisphere glaciation (3–2 MA). *Paleoceanography*, *7*(5), 645–672. https://doi.org/10.1029/92PA01609

Rea, D. K., Snoeckx, H., & Joseph, L. H. (1998). Late Cenozoic Eolian deposition in the North Pacific: Asian drying, Tibetan uplift, and cooling of the northern hemisphere. *Paleoceanography*, *13*(3), 215–224. https://doi.org/10.1029/98PA00123

Ritchie, J. C., Eyles, C. H., & Haynes, C. V. (1985). Sediment and pollen evidence for an early to mid-Holocene humid period in the eastern Sahara. *Nature*, *314*(6009), 352–355. https://doi.org/10.35619/ucpmk.vi27.44

Rose, C., Polissar, P. J., Tierney, J. E., Filley, T., de Menocal, P. B., & de Menocal, P. B. (2016). Changes in northeast African hydrology and vegetation associated with Pliocene-Pleistocene sapropel cycles. *Philosophical Transactions of the Royal Society B: Biological Sciences*, *371*(1698), 20150243. https://doi.org/10.1098/rstb.2015.0243

Rossignol-Strick, M. (1983). African monsoons, an immediate climate response to orbital insolation. *Nature*, *304*(5921), 46–49. https://doi.org/10.1038/304046a0

Rossignol-Strick, M. (1985). Mediterranean Quaternary sapropels, an immediate response of the African monsoon to variation of insolation. *Palaeogeography, Palaeoclimatology, Palaeoecology*, *49*(3–4), 237–263. https://doi.org/10.1016/0031-0182(85)90056-2

Rozanski, K., Araguás-Araguás, L., & Gonfiantini, R. (1993). Isotopic patterns in modern global precipitation. *Climate Change in Continental Isotopic Records*, *78*, 1–36. https://doi.org/10.1029/gm078p0001

Ruddiman, W. F., Sarnthein, M., Backman, J., Baldauf, J., Curry, W., Dupont, L., et al. (1989). Late miocene to pleistocene evolution of climate in Africa and the low-latitude Atlantic: Overview of leg 108 results. *Proceedings of the Ocean Drilling Program, Scientific Results, ODP, Leg 108, Eastern Tropical Atlantic*, *108*, 463–484. https://doi.org/10.2973/odp.proc.sr.108.173.1989

Sachse, D., Billault, I., Bowen, G. J., Chikaraishi, Y., Dawson, T. E., Feakins, S. J., et al. (2012). Molecular paleohydrology: Interpreting the hydrogen-isotopic composition of lipid biomarkers from photosynthesizing organisms. *Annual Review of Earth and Planetary Sciences*, *40*(1), 221–249. https://doi.org/10.1146/annurev-earth-042711-105535

Salzmann, U., Haywood, A. M., Lunt, D. J., Valdes, P. J., & Hill, D. J. (2008). A new global biome reconstruction and data-model comparison for the Middle Pliocene. *Global Ecology and Biogeography*, *17*(3), 432–447. https://doi.org/10.1111/j.1466-8238.2008.00381.x

Sankaran, M., Hanan, N. P., Scholes, R. J., Ratnam, J., Augustine, D. J., Cade, B. S., et al. (2005). Determinants of woody cover in African savannas. *Nature*, *438*(7069), 846–849. https://doi.org/10.1038/nature04070

Schefuß, E., Schouten, S., Jansen, J. H. F., & Sinninghe Damsté, J. S. (2003). African vegetation controlled by tropical sea surface temperatures in the mid-Pleistocene period. *Nature*, *422*(6930), 418–421. https://doi.org/10.1038/nature01500

Schrag, D. P., Adkins, J. F., McIntyre, K., Alexander, J. L., Hodell, D. A., Charles, C. D., & McManus, J. F. (2002). The oxygen isotopic composition of seawater during the Last Glacial Maximum. *Quaternary Science Reviews*, *21*(1–3), 331–342. https://doi.org/10.1016/S0277-3791(01)00110-X

Skonieczny, C., Bory, A., Bout-Roumazeilles, V., Abouchami, W., Galer, S. J. G., Crosta, X., et al. (2011). The 7–13 March 2006 major Saharan outbreak: Multiproxy characterization of mineral dust deposited on the West African margin. *Journal of Geophysical Research*, *116*(D18), D18210. https://doi.org/10.1029/2011JD016173

Skonieczny, C., Bory, A., Bout-Roumazeilles, V., Abouchami, W., Galer, S. J. G., Crosta, X., et al. (2013). A three-year time series of mineral dust deposits on the West African margin: Sedimentological and geochemical signatures and implications for interpretation of marine paleo-dust records. *Earth and Planetary Science Letters*, *364*, 145–156. https://doi.org/10.1016/j.epsl.2012.12.039

Skonieczny, C., McGee, D., Winckler, G., Bory, A., Bradtmiller, L. I., Kinsley, C. W., et al. (2019). Monsoon-driven Saharan dust variability over the past 240,000 years. *Science Advances*, *5*(1), eaav1887. https://doi.org/10.1126/sciadv.aav1887

Sosdian, S. M., Greenop, R., Hain, M. P., Foster, G. L., Pearson, P. N., & Lear, C. H. (2018). Constraining the evolution of Neogene ocean carbonate chemistry using the boron isotope pH proxy. *Earth and Planetary Science Letters*, *498*, 362–376. https://doi.org/10.1016/j.epsl.2018.06.017

Staver, A. C., Archibald, S., & Levin, S. A. (2011). The global extent and determinants of savanna and forest as alternative biome states. *Science*, *334*(6053), 230–232. https://doi.org/10.1126/science.1210465

Stevens, N., Erasmus, B. F. N., Archibald, S., & Bond, W. J. (2016). Woody encroachment over 70 years in South African savannahs: Overgrazing, global change or extinction aftershock? *Philosophical Transactions of the Royal Society B: Biological Sciences*, *371*(1703), 20150437. https://doi.org/10.1098/rstb.2015.0437

Stuut, J.-B., Zabel, M., Ratmeyer, V., Helmke, P., Schefuß, E., Lavik, G., & Schneider, R. (2005). Provenance of present-day eolian dust collected off NW Africa. *Journal of Geophysical Research*, *110*(D4), D04202. https://doi.org/10.1029/2004JD005161

Tachikawa, K., Rapuc, W., Vidal, L., Dubois-Dauphin, Q., Westerhold, T., Guihou, A., et al. (2021). Eastern Atlantic deep-water circulation and carbon storage inferred from neodymium and carbon isotopic compositions over the past 1.1 million years. *Quaternary Science Reviews*, *252*, 106752. https://doi.org/10.1016/j.quascirev.2020.106752

Tiedemann, R., Sarnthein, M., & Shackleton, N. J. (1994). Astronomic timescale for the pliocene Atlantic $\delta^{18}O$ and dust flux records of ocean drilling program site 659. *Paleoceanography*, *9*(4), 619–638. https://doi.org/10.1029/94PA00208

Tjallingii, R., Claussen, M., Stuut, J.-B. W., Fohlmeister, J., Jahn, A., Bickert, T., et al. (2008). Coherent high- and low-latitude control of the northwest African hydrological balance. *Nature Geoscience*, *1*(10), 670–675. https://doi.org/10.1038/ngeo289

Trauth, M. H., Larrasoaña, J. C., & Mudelsee, M. (2009). Trends, rhythms and events in Plio-Pleistocene African climate. *Quaternary Science Reviews*, *28*(5–6), 399–411. https://doi.org/10.1016/J.QUASCIREV.2008.11.003

Tuenter, E., Weber, S. L., Hilgen, F. J., Lourens, L. J., & Ganopolski, A. (2005). Simulation of climate phase lags in response to precession and obliquity forcing and the role of vegetation. *Climate Dynamics*, *24*(2–3), 279–295. https://doi.org/10.1007/s00382-004-0490-1

Vallé, F., Dupont, L. M., Leroy, S. A. G. G., Schefuß, E., & Wefer, G. (2014). Pliocene environmental change in West Africa and the onset of strong NE trade winds (ODP Sites 659 and 658). *Palaeogeography, Palaeoclimatology, Palaeoecology*, *414*, 403–414. https://doi.org/10.1016/j.palaeo.2014.09.023

van der Does, M., Brummer, G. J. A., van Crimpen, F. C. J., Korte, L. F., Mahowald, N. M., Merkel, U., et al. (2020). Tropical rains controlling deposition of Saharan dust across the North Atlantic Ocean. *Geophysical Research Letters*, *47*(5), 1–10. https://doi.org/10.1029/2019GL086867

Venz, K. A., & Hodell, D. A. (2002). New evidence for changes in Plio–pleistocene deep water circulation from Southern Ocean ODP leg 177 site 1090. *Palaeogeography, Palaeoclimatology, Palaeoecology*, *182*(3–4), 197–220. https://doi.org/10.1016/S0031-0182(01)00496-5

Vogts, A., Schefuß, E., Badewien, T., & Rullkötter, J. (2012). *n*-Alkane parameters from a deep sea sediment transect off southwest Africa reflect continental vegetation and climate conditions. *Organic Geochemistry*, *47*, 109–119. https://doi.org/10.1016/j.orggeochem.2012.03.011

Voss, K. K., & Evan, A. T. (2020). A new satellite-based global climatology of dust aerosol optical depth. *Journal of Applied Meteorology and Climatology*, *59*(1), 83–102. https://doi.org/10.1175/JAMC-D-19-0194.1

Wara, M. W., Ravelo, A. C., & Delaney, M. L. (2005). Climate change: Permanent El Niño-like conditions during the pliocene Warm Period. *Science*, *309*(5735), 758–761. https://doi.org/10.1126/science.1112596

Weiffenbach, J. E., Baatsen, M. L. J., Dijkstra, H. A., Von Der Heydt, A. S., Abe-Ouchi, A., Brady, E. C., et al. (2023). Unraveling the mechanisms and implications of a stronger mid-Pliocene Atlantic meridional overturning circulation (AMOC) in PlioMIP2. *Climate of the Past*, *19*(1), 61–85. https://doi.org/10.5194/cp-19-61-2023

Westerhold, T., Marwan, N., Drury, A. J., Liebrand, D., Agnini, C., Anagnostou, E., et al. (2020). An astronomically dated record of Earth's climate and its predictability over the last 66 million years. *Science*, *369*(6509), 1383–1387. https://doi.org/10.1126/science.aba6853

White, F. (1983). *The vegetation of Africa* (Vol. 20). Natural Resources Research, UNESCO.

Winckler, G., Anderson, R. F., & Schlosser, P. (2005). Equatorial Pacific productivity and dust flux during the mid-Pleistocene climate transition. *Paleoceanography*, *20*(4), 1–10. https://doi.org/10.1029/2005PA001177

Yamamoto, M., Clemens, S. C., Seki, O., Tsuchiya, Y., Huang, Y., O'ishi, R., & Abe-Ouchi, A. (2022). Increased interglacial atmospheric CO_2 levels followed the mid-Pleistocene Transition. *Nature Geoscience*, *15*(April), 307–313. https://doi.org/10.1038/s41561-022-00918-1

Yehudai, M., Kim, J., Pena, L. D., Jaume-Segui, M., Knudson, K. P., Bolge, L., et al. (2021). Evidence for a Northern Hemispheric trigger of the 100,000-y glacial cyclicity. *Proceedings of the National Academy of Sciences of the United States of America*, *118*(46). https://doi.org/10.1073/pnas.2020260118

Zhang, R., Jiang, D., Zhang, Z., Yan, Q., & Li, X. (2019). Modeling the late Pliocene global monsoon response to individual boundary conditions. *Climate Dynamics*, *53*(7–8), 4871–4886. https://doi.org/10.1007/s00382-019-04834-w

References From the Supporting Information

Chiapello, I., Bergametti, G., Gomes, L., Chatenet, B., Dulac, F., Pimenta, J., & Suares, E. S. (1995). An additional low layer transport of Sahelian and Saharan dust over the north-eastern Tropical Atlantic. *Geophysical Research Letters*, *22*(23), 3191–3194. https://doi.org/10.1029/95GL03313

Eggleston, S., Schmitt, J., Bereiter, B., Schneider, R., & Fischer, H. (2016). Evolution of the stable carbon isotope composition of atmospheric CO_2 over the last glacial cycle. *Paleoceanography*, *31*(3), 434–452. https://doi.org/10.1002/2015PA002874

Ellis, L., & Fincannon, A. L. (1998). Analytical improvements in irm-GC/MS analyses: Advanced techniques in tube furnace design and sample preparation. *Organic Geochemistry*, *29*(5–7–7 pt 2), 1101–1117. https://doi.org/10.1016/S0146-6380(98)00157-0

Feng, J.-L., Zhu, L.-P., Zhen, X.-L., & Hu, Z.-G. (2009). Grain size effect on Sr and Nd isotopic compositions in eolian dust: Implications for tracing dust provenance and Nd model age. *Geochemical Journal*, *43*(2), 123–131. https://doi.org/10.2343/geochemj.1.0007

Mazeas, L., Budzinski, H., & Raymond, N. (2002). Absence of stable carbon isotope fractionation of saturated and polycyclic aromatic hydrocarbons during aerobic bacterial biodegradation. *Organic Geochemistry*, *33*(11), 1259–1272. https://doi.org/10.1016/S0146-6380(02)00136-5

Risi, C., Bony, S., & Vimeux, F. (2008). Influence of convective processes on the isotopic composition ($\delta^{18}O$ and δD) of precipitation and water vapor in the tropics: 2. Physical interpretation of the amount effect. *Journal of Geophysical Research*, *113*(19), D19306. https://doi.org/10.1029/2008JD009943

Risi, C., Bony, S., Vimeux, F., Descroix, L., Ibrahim, B., Lebreton, E., et al. (2008). What controls the isotopic composition of the African monsoon precipitation? Insights from event-based precipitation collected during the 2006 AMMA field campaign. *Geophysical Research Letters*, *35*(24), L24808. https://doi.org/10.1029/2008GL035920

Tierney, J. E., & de Menocal, P. B. (2013). Abrupt shifts in Horn of Africa hydroclimate since the last glacial maximum. *Science*, *342*(6160), 843–846. https://doi.org/10.1126/science.1240411

Tipple, B. J., & Pagani, M. (2007). The early origins of terrestrial C_4 photosynthesis. *Annual Review of Earth and Planetary Sciences*, *35*(1), 435–461. https://doi.org/10.1146/annurev.earth.35.031306.140150

Vogts, A., Moossen, H., Rommerskirchen, F., & Rullkötter, J. (2009). Distribution patterns and stable carbon isotopic composition of alkanes and alkan-1-ols from plant waxes of African rain forest and savanna C3 species. *Organic Geochemistry*, *40*(10), 1037–1054. https://doi.org/10.1016/J.ORGGEOCHEM.2009.07.011

Wakeham, S. G., & Pease, T. K. (2004). Lipid analysis in marine particle and sediment samples (p. 33).

Worden, J., Noone, D., Bowman, K., T. T. E. S. Science Team and Data Contributors, Beer, R., Eldering, A., et al. (2007). Importance of rain evaporation and continental convection in the tropical water cycle. *Nature*, *445*(7127), 528–532. https://doi.org/10.1038/nature05508

Yamamoto, S., & Kawamura, K. (2012). Application of urea adduction technique to polluted urban aerosols for the determination of hydrogen isotopic composition of n-alkanes. *International Journal of Environmental Analytical Chemistry*, *92*(3), 302–312. https://doi.org/10.1080/03067310903045505

Yan, Y., Bender, M. L., Brook, E. J., Clifford, H. M., Kemeny, P. C., Kurbatov, A. V., et al. (2019). Two-million-year-old snapshots of atmospheric gases from Antarctic ice. *Nature*, *574*(7780), 663–666. https://doi.org/10.1038/s41586-019-1692-3